University of Nottingham
UK | CHINA | MALAYSIA

EEE Department of Electrical and Electronic Engineering

EEEE4129 (SUM1 22-23): MSc Project

AI and fly brains – tools to study pain and aversive learning in fruit flies

AUTHOR: **Mr Hamza Bin Mazhar**

ID NUMBER: **20498276**

SUPERVISOR: **Dr. Kevin Webb**

MODERATOR: **Dr. Paul Blunt**

DATE: **04 Sep 2023**

MSc Project Thesis is submitted in part fulfilment of the requirements of the degree of MSc in Electronic Communications and Computer Engineering.

Table of Contents

1 Introduction

Behavioural annotation of animals in labs involves the systematic observation and recording of their actions, reactions, and interactions to better understand their behaviour, cognition, and responses to various stimuli. This process contributes to scientific research, particularly in fields such as psychology, neuroscience, ethology, and pharmacology. Researchers design experiments to investigate specific behaviours or responses of animals. This may involve exposing animals to controlled conditions or stimuli, such as mazes, puzzles, social interactions, or sensory experiences.

Skilled researchers or trained personnel observe animals while they interact with their environment, other animals, or stimuli. Observations can be done in real-time or recorded for later analysis.

Various methods are used to record animal behaviours, including video cameras, audio recordings, computer software, and written notes. These recordings capture details such as movement patterns, vocalisations, postures, and interactions as shown in Figure 1. The recorded data is then annotated, which involves labelling and categorising behaviours based on predefined criteria. Annotations might include identifying specific actions (e.g., grooming, exploring, mating), body language (e.g., aggression, fear), and responses to stimuli (e.g., approach, avoidance, escape locomotion). Analysing annotated data allows researchers to draw conclusions about the animals' behaviours, emotional states, cognitive abilities, and responses to experimental conditions.

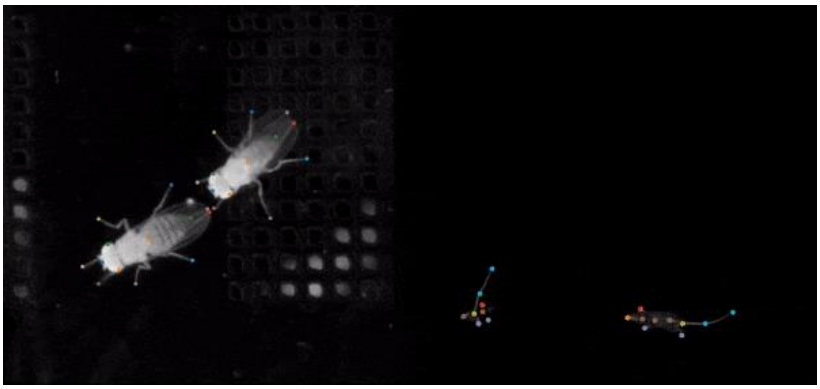

Figure 1. Animal Pose Tracking using SLEAP [1]

Behavioural annotation provides insights into natural behaviour patterns, social interactions, learning, memory, and other cognitive processes. This foundational knowledge contributes to a better understanding of species-specific behaviours and their evolutionary significance. Studying animal behaviour helps explore neural mechanisms, brain functions, and the effects of various manipulations on behaviour. This contributes to our understanding of human brain function and mental disorders. Behavioural annotation is used to assess the effects of drugs, chemicals, or substances on animals' behaviour, helping determine potential therapeutic benefits or adverse effects. It can uncover insights into the ethology of animals.

1.1 Existing Functional Models in the *Drosophila* Lab

As of now, in the *Drosophila* lab at The University of Nottingham, manual annotation of *Drosophila* larval behaviours is conducted as part of various research studies. Research is carried out *in vivo* real-time physiology in the *Drosophila* brain. These stimuli can either be mechanical (mechanically pricking them), chemical (concentrated HCL solution) or optical (shining LEDs on *Drosophila* larvae). After stimulation, the larvae present a behaviour called NEL (Nociceptive Escape Locomotion) characterised by body-rolling and twisting shown in Figure 2.

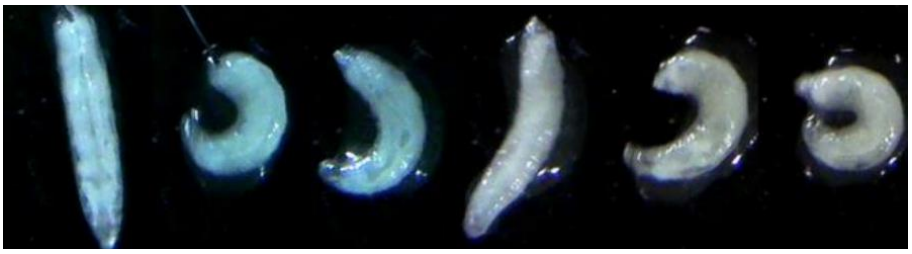

Figure 2. Drosophila Larvae exhibiting NEL.

Currently, this is annotated by humans by watching through a microscope. The major problem with this method is a low throughput and latency issues. Another problem is the subjectivity whilst a person is performing this experiment. What one person may think is an NEL, another person might have a different opinion. This project aims at developing a workflow for data extraction from high contrast videos of experiments on *Drosophila* based on behavioural responses to stimulation.

Therefore, the ultimate objective of this thesis is to automate the whole procedure using novel AI techniques to perform real time behavioural annotation. This helps remove the subjectivity and introduces a truly autonomous system that can give us real-time, low latency results. This whole thesis lies in a pipeline meant for screening work in the selection of novel drugs to study the aversive behaviour of larva. This will help in collecting videos from multi-well petri-dish plates, thereby assuring a high degree of parallelisation for all the experiments, which can be analysed and compared as fast as possible.

The establishment of a data extraction workflow from *Drosophila* larvae experiment videos holds immense importance for future researchers, enabling them to efficiently gather and analyse extensive behavioural datasets. Additionally, a key objective is to craft a workflow that is reproducible, ensuring that should someone wish to train another model using comparable methods or parameters in the future, it can be accomplished with ease. This approach also underscores the iterative nature of the pipeline, facilitating the retraining of models when necessary whilst keeping optimal parameters constant and variating suboptimal parameters. Thus, when the lens is decided to be optimal for experiment video collection (~35 mm – 100 mm as in section 3.2.1), it can be kept constant. Next up are the illumination conditions can be altered to make sure that they conform to the range that does not stimulate the optogenetics (~850 nm wavelength illumination as in section 3.7.2). Once set they can be comparatively analysed with the exposure time and values, contrast, and saturation to ensure the dark field video collections. This helps setup an environment making it certain that there are some parameters in the final prototype that prove to be better at performing these tasks than others.

1.2 Reasons for using *Drosophila* Larvae

For the past century, *Drosophila melanogaster*, commonly referred to as the fruit fly, has remained the preferred model system for numerous researchers [2]. Its enduring prominence as a model organism has facilitated the establishment of a diverse array of techniques, both tried-and-true and novel, aimed at unravelling a multitude of scientific inquiries. The rich tradition surrounding

Drosophila research has paved the way for the development and refinement of a toolkit that continues to be leveraged to address a wide spectrum of scientific questions.

Recent advancements in the realm of techniques have further underscored the dynamic nature of *Drosophila* research. Two notable breakthroughs stand out: the introduction of methods enabling the targeted reduction of gene expression through RNA interference and the ability to replace genes via homologous recombination [3]. These advancements illustrate the ongoing commitment to expanding the repertoire of technical methodologies available to researchers who are deeply engaged with *Drosophila* investigations. By harnessing the power of RNA interference, scientists can effectively "knockdown" specific genes, enabling the study of their functions and roles in various biological processes. Similarly, the capability to replace genes through homologous recombination not only unveils the intricate workings of individual genes but also offers insights into broader genetic mechanisms [4].

This continuous refinement and diversification of techniques in *Drosophila* research reflect the collective pursuit of enhancing our grasp of fundamental biological principles.

1.2.1 Model for Genome Analysis

Drosophila larva is a simple model organism with features that make it ideal for studying the neurobiology of behaviour [5]. The simplicity of *Drosophila* larvae makes understanding and exploring associative plasticity on a synaptic level a feasible task. Notably, this organism manifests congruence in approximately 75% of human disease-associated genes, further accentuating its relevance in translational research in human neurobiology. In the lab, the larvae are exposed to noxious stimuli [6].

Fruit fly larvae have played a pivotal role in advancing our comprehension of genetics, development, behaviour, and various biological processes. *Drosophila* larvae are preferred for experimentation due to their well-characterised genome, short life cycle as shown in Figure 3, and the ability to manipulate specific genes using techniques like genetic crosses, RNA interference

(RNAi), and genome editing (CRISPR-Cas9). This facilitates the investigation of gene functions and their roles in diverse processes. Additionally, the conservation of biological processes across species means that insights gained from studying *Drosophila* larvae often hold relevance for other organisms, including humans. The larvae's relatively simple nervous system and distinct behaviours make them valuable for studying neurobiology and behaviour [7].

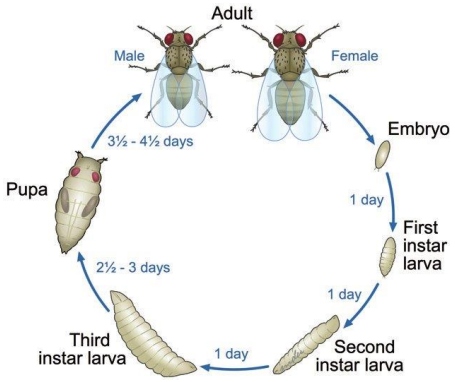

Figure 3. Life Cycle of Fruit Fly Larvae [8].

Furthermore, their developmental stages, from larva to pupa and adult, provide an excellent model for studying organ formation, tissue differentiation, and metamorphosis. With a high reproductive rate, ease of handling, and cost-effectiveness, *Drosophila* larvae enable researchers to conduct high-throughput experiments and large-scale genetic screens. Overall, the versatile nature, genetic manipulability, and physiological significance of *Drosophila* larvae make them invaluable tools for unravelling a diverse array of biological inquiries, thus enriching our understanding of fundamental biological processes and their implications for human health [9].

This larva’s genome comprises approximately 15,500 genes distributed across its four chromosomes, which, when compared to humans with about 22,000 genes scattered throughout 23 chromosomes, results in a higher gene density per chromosome in *Drosophila*. This compact genome organisation contributes to making *Drosophila* species exceptionally amenable to scientific investigation. Just as humans inherit traits and genetic information from their ancestors, fruit flies pass down traits across generations, thereby providing with an avenue to study inheritance patterns

akin to those observed in humans [10]. The exploration of these traits across various *Drosophila* lineages enables scientists to extrapolate and infer genetic trends pertinent to the human context.

The extensive research conducted on *Drosophila* offers foundational insights into the transmission of genes across a spectrum of organisms, illuminating the fundamental rules governing genetic inheritance. Furthermore, *Drosophila* serves as an indispensable *in vivo* tool for scrutinising complex conditions like Alzheimer's disease [11]. Intriguingly, certain biological elements initially identified in *Drosophila*, such as “rhomboid proteases,” have exhibited a remarkable degree of conservation across different life forms, including eukaryotes, mitochondria, and even bacteria [12].

Moreover, the melanin pigment present in *Drosophila* has been extensively studied for its ability to shield DNA against the damaging effects of ionising radiation. The cumulative findings from diverse research avenues in *Drosophila* not only deepen our comprehension of these creatures but also offer a broader understanding of genetics, biology, and the intricate molecular mechanisms that underpin life across the biological spectrum [13].

This study opens avenues for advancing our understanding of modelling pain receptors and neural connections in humans. The primary reason behind this is their significance as a genetic analysis model for studying hypersensitivity of pain receptors.

1.2.2 Ethical Considerations

The principles of ethical treatment of animals in scientific research, commonly referred to as the "4 Rs" are an expansion of the earlier "3 Rs" principles, which were introduced by Russell and Burch in 1959 [14].

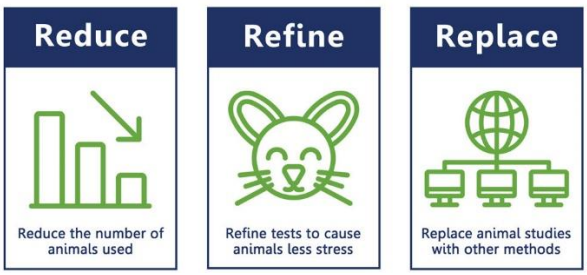

Figure 4. The 3R's of Animal Research (extracted from link).

The 4 Rs stand for Reduction, Refinement, Replacement, and Responsibility, and they guide the ethical use of animals in research:

1. Reduction: This principle puts an emphasis on minimising the number of animals used in experiments to the lowest possible level while still obtaining reliable and meaningful results. Researchers achieve this by utilising advanced experimental design, thorough literature reviews to avoid duplicating experiments, applying statistical analysis that allows for smaller sample sizes, and sharing data and resources.
2. Refinement: Refinement aims to enhance the well-being of animals involved in experiments by reducing any pain, distress, or suffering they might experience. Improvements in living conditions, proper training for handling animals, the use of anaesthesia and analgesia when appropriate, and humane euthanasia to minimise suffering at the end of experiments fall under this principle.
3. Replacement: This principle encourages finding alternative methods that eliminate or reduce the need for using animals in experiments. In silico methods, which involve computer simulations and modelling, as well as in vitro techniques like cell and tissue culture testing, are examples of approaches that can replace the use of live animals. Additionally, certain non-vertebrate organisms can be used in place of higher animals when feasible.
4. Responsibility: The fourth "R" highlights the broader ethical responsibilities that researchers, institutions, and society have toward animals used in experiments. This includes promoting animal welfare by considering animals' social well-being, developing scientific methods to assess their sentience, pain perception, consciousness, and intelligence, and engaging in meaningful discussions about animal ethics in the public sphere.

These principles provide a framework for evaluating and conducting research that involves animals, ensuring that ethical considerations are considered at every stage of the research process. The 4 Rs principles are intended to balance scientific progress with ethical treatment of animals, promoting the advancement of knowledge while minimising harm and respecting the intrinsic value of animal life.

The utilisation of *Drosophila* larvae in scientific research can be justified in accordance with the principles of these 4Rs:

1. Reduction: *Drosophila* larvae, due to their fast reproductive cycle and genetic homogeneity, offer a valuable model system for researchers. Their ability to provide meaningful insights with relatively small sample sizes aligns with the Reduction principle. By using *Drosophila* larvae, researchers can reduce the number of experimental animals required while still obtaining reliable and significant data. The larvae's short lifespan allows for efficient experimental designs that yield valuable results without the need for large-scale studies involving higher animals.

2. Refinement: When it comes to Refinement, *Drosophila* larvae provide an advantageous platform to minimise harm and distress. These organisms are small and amenable to carefully controlled experimental conditions. Researchers can ensure a high level of welfare by precisely controlling factors such as temperature, humidity, and nutrition, thereby minimising any potential stress or discomfort. Furthermore, the larvae's size enables the administration of substances or procedures with minimal invasiveness, reducing the potential for pain and suffering.

3. Replacement: *Drosophila* larvae also align with the replacement principle by serving as an alternative to higher animals in various experiments. Their genetic similarities to higher organisms, along with the availability of advanced techniques such as in vitro cell cultures and genetic manipulation, enable researchers to explore hypotheses and gather data without

resorting to experiments on more complex vertebrate animals. In cases where the research question can be addressed using *Drosophila* larvae, these organisms offer a valid replacement option that aligns with ethical considerations.

4. Responsibility: Lastly, the use of *Drosophila* larvae demonstrates Responsibility in animal research. As part of this principle, researchers and the scientific community are called upon to consider animal welfare, ethical implications, and societal perceptions. *Drosophila* larvae provide an opportunity to responsibly engage in research while minimising harm to animals. Advances in our understanding of larval biology contribute to the broader discourse on animal ethics and welfare, as researchers actively work towards refining methods, assessing sentience, and applying ethical considerations to their work [15].

2 Literature Review

2.1 *Drosophila* as a Model for Nociception Studies

Nociception refers to the perception of potentially damaging stimuli that can harm tissues. In the case of *Drosophila,* nociceptive sensory neurons possess a single axon and one or more dendrites. Among larval flies, two primary types of peripheral sensory neurons exist beneath the protective epidermis barrier, known as type I and type II neurons. These neurons are categorised based on their dendrite count and anatomical features [16].

Type I neurons are associated with bristle-type and chordotonal sensory organs. They feature a single ciliated dendrite primarily responsible for mechanical sensory functions such as light touch. In contrast, type II neurons extend multiple dendritic branches, reaching nearly every epidermal cell in the larval barrier epidermis. They are often referred to as multidendritic (md) sensory neurons or dendritic arborization (DA) neurons. Interestingly, they bear a structural resemblance to mammalian nociceptors [17].

When the gene activity in md neurons is suppressed, larvae become entirely unresponsive to noxious stimuli, highlighting the crucial role of these neurons in generating responses to harmful stimuli. This evidence underscores the functional significance of md sensory neurons as nociceptors Furthermore, studies examining the morphology of type II neurons have revealed their diversity, identifying at least four subtypes.

These neurons are collectively referred to as class I-IV neurons and cover the larval body wall. Class I neurons have the simplest dendritic domains, while class IV neurons exhibit the most intricate structures.

Class I neurons project to the motor nerve stacks of ventral dorsal ganglia, likely providing feedback to motor neurons. On the other hand, class II, class III, and class IV neurons all project to the ventral nerve pile and are expected, based on analogies with other insects, to serve somatosensory

functions [18]. Class I neurons play a pivotal role in coordinating the precise timing of peristaltic locomotion [19]. Both Class II and Class III neurons contribute to responses triggered by gentle contacts, with type III neurons taking the lead. Class III neurons are also implicated in mechanical nociception and cold nociception. Morphologically resembling mammalian nociceptors, Class IV neurons exhibit polymodal sensitivity to various sensory stimuli [20]. When Class IV neurons are ablated or silenced, larval responses to noxious stimuli are significantly reduced, while activating these neurons induces a corkscrew-like rolling behaviour to noxious stimuli [17]. These peripheral nervous system neurons are responsible for detecting multiple nociceptive modalities, including mechanical force, harmful heat, low-wavelength light, and chemical cues, achieved through distinct receptors.

Much of the ongoing research into pain in Drosophila focuses on nociception, which is analogous to acute pain in mammals. In response to noxious stimuli, multiple pathways are activated in md neurons.

Following the perception of acute pain, md neurons often contribute to the development of allodynia and hyperalgesia. Diverse pathways associated with these phenomena are also present in md neurons. Hedgehog (Hh) signalling, for example, contributes to allodynia and hyperalgesia in response to UV light exposure in *Drosophila* larvae. Hh signalling collaborates with tumour necrosis factor (TNF) signalling to mediate allodynia and several TRP channels mentioned earlier participate in allodynia and hyperalgesia downstream of these pathways. Painless is crucial for the development of Hh- or TNF-induced thermal hyperalgesia, while dTRPA1 is vital for Hh-induced thermal hyperalgesia. The BMP pathway is active in md neurons during allodynia and hyperalgesia, acting downstream of the Hh signalling pathway [21]. Moreover, the Decapentaplegic (Dpp, the ortholog of mammalian bone morphogenetic protein 2/4) and its downstream signalling pathways have been shown to be required for inducing allodynia in *Drosophila* md neurons. These studies emphasise that during painful events, interconnected pain signalling pathways in *Drosophila* md neurons

collaboratively engage in acute nociception and subsequent chronic pain states (allodynia and hyperalgesia)[22].

2.2 Advancing Anti-Pain Medications through *Drosophila* Model Research

Drosophila melanogaster serves as a widely employed organism in genetic research and has also found application in the realm of drug discovery. The utilisation of *Drosophila* for drug screening presents distinct advantages, including its economical maintenance, prolific reproductive capabilities, and swifter screening procedures compared to traditional rat models. These attributes render it particularly invaluable for the exploration of novel pain-relief medications, particularly those linked to shared pain-related genes and responses that align with human physiology [23].

Numerous techniques are available for administering drugs to fruit flies. These encompass vapor exposure methods, the incorporation of drugs into their food or onto filter paper soaked in drug-infused [24], direct injection onto the exposed nerve cord of decapitated flies, and abdominal injection to facilitate rapid diffusion throughout the organism. Additionally, the capacity for high-throughput screening through random mutations or targeted RNAi-mediated knockdown enables the identification of new drugs and targets [17].

Consequently, the *Drosophila* fly model holds considerable promise for the screening of potential analgesic compounds and the discovery of novel drugs. This approach has gained significant attention among researchers involved in pharmacological investigations of pain. Conversations concerning pain in animals inevitably encompass anthropomorphic interpretations. From a pragmatic standpoint, comprehending an animal's reaction to noxious stimuli and the potential for drug interventions to alleviate this response constitute pivotal aspects of pain-related research.

The peptide Tv1, derived from *Terebra variegata*, has displayed notable antinociceptive effects in mature flies when introduced through injection, effectively reducing their sensitivity to harmful heat stimuli [25].

Three analogues of anaesthetics target the same site as halothane, leading to a reduction in heat sensitivity in flies exposed to intense light-induced heating [26]. These analogues are as follow:

1. Enflurane
2. Isoflurane
3. Desflurane

Paclitaxel, a commonly used chemotherapy agent, induces chronic nociception. Exposure of larval nociceptive systems in fruit flies to paclitaxel results in a substantial and dose-dependent escalation of aversive escape responses during noxious thermal stimuli [27].

2.3 Channelrhodopsins for optogenetics

Optogenetics has gained widespread popularity as a tool for precise neuron activation, offering exceptional spatiotemporal precision. Optogenetics builds upon the discovery that opsins, light-sensitive molecules, can be expressed within neurons. These neurons, sensitive to light, can be precisely manipulated with light, offering temporal and spatial precision that aligns with the brain's natural processing. The engineering of opsins for optogenetic applications is an ever-evolving field, continually providing new and significantly modified opsins to cater to diverse research applications, including those involving primates and humans [28].

The initial isolation and examination of Channelrhodopsin ChR2 was conducted by Georg Nagel, Ernst Bamberg, and Peter Hegemann. Their research aimed to identify the proteins responsible for generating photocurrents in the single-celled green alga *Chlamydomonas reinhardtii*. Subsequently, Ed Boyden, Feng Zhang, and Karl Deisseroth, in partnership with Nagel and Bamberg, took this discovery a step further. They repurposed ChR2, originally conceived as a sensor, and demonstrated its potential as an actuator. Their groundbreaking work illustrated that this light-gated channel could effectively regulate neural activity with exceptional temporal precision. ChR2 induces calcium influx at specific light wavelengths (450–490 nm) to manipulate neural activity [29].

Various channelrhodopsin variants like Chronos, VChR1, C1V1, ReaChR, and Chrimson have since emerged to selectively affect different neurons, depolarising them. This enables testing specific neuron functions within circuits, assessing behavioural responses, and functional connectivity alongside calcium indicators.

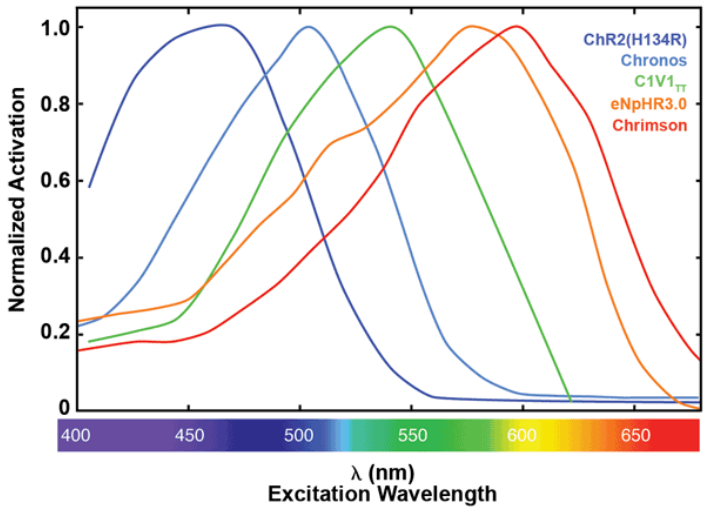

Figure 5. Graphs showing the normalised activation profiles of various Opsins(extracted from link).

Opsins can be categorised based on their effect on neuronal activity, meaning whether they primarily activate or inhibit the activity of neurons. Additionally, they exhibit spectral sensitivity, which refers to the range of wavelengths of light to which they respond. This sensitivity is not uniform but rather has specific peak wavelengths at which opsins are most responsive, and an interval that defines the range of wavelengths over which they maintain some level of responsiveness. They also employ different means of ion transport across the cell membrane. Some utilise ion channels, allowing ions to flow freely upon exposure to light, while others employ ion pumps, actively transporting ions across the membrane. Furthermore, opsins differ in their kinetics, which describe how quickly they respond to light (activation) and return to their inactive state (deactivation) when the light stimulus is removed. Finally, they exhibit varying photocurrent properties, producing different levels of electrical currents in response to light stimulation. In Figure 5, it is visually represented that most opsins can respond to a wide range of light wavelengths. Within this broad range, there is a specific interval where opsins display their highest sensitivity, resulting in the

generation of maximum activation and photocurrent. Light-activated proteins used in optogenetics applications typically have peak excitation wavelengths within the visible or infrared spectrum.

For instance, Channelrhodopsin-2 (ChR2) is most sensitive to blue light, with its peak activation occurring around 470 nm. Conversely, Chrimson, the opsin utilised in this particular study, is activated by red light, with a peak activation wavelength of approximately 600 nm.

2.4 Camera Architectures for video collection

2.4.1 Sensor Architecture and Photodetection in a CMOS Active Pixel Sensor

At the heart of a camera lies the image sensor, a grid-like array of individual light-sensitive sites known as pixels. In an active pixel design, each pixel incorporates its own signal processing circuitry, typically including amplification and readout components. This contrasts with passive pixel sensors, where the pixel merely accumulates charge in response to light but lacks built-in processing capabilities. Each pixel incorporates an intricate arrangement of diode circuits and a capacitor. CMOS (Complementary Metal-Oxide-Semiconductor) photodetectors function by utilising a PN-junction photodiode as their core component. When this photodiode is reverse-biased, meaning a voltage is applied in a way that the P-side of the junction becomes more negative relative to the N-side (while staying below the breakdown voltage), it allows a current to flow through the diode. This current is directly proportional to the intensity of incident light and is commonly referred to as the photo current.

When the exposure phase begins, the transfer gate is briefly opened, allowing the charge generated by incoming photons striking the photodiode to flow to the diffusion node. The diffusion node, often referred to as the floating diffusion (FD), is a key element in the pixel structure. It is typically a region of the silicon substrate that is electrically isolated (floating) from other parts of the pixel. The transfer node is often represented by a component called the transfer gate (TG). The primary function of the transfer node is to control the movement of electrical charge from the photodetector (PD) to the floating diffusion (FD) during the exposure phase, thereby decreasing the voltage present at the node.

This voltage at the FD represents the pixel's response to the light. The voltage is then amplified and then passed through an Analog-to-Digital converter.

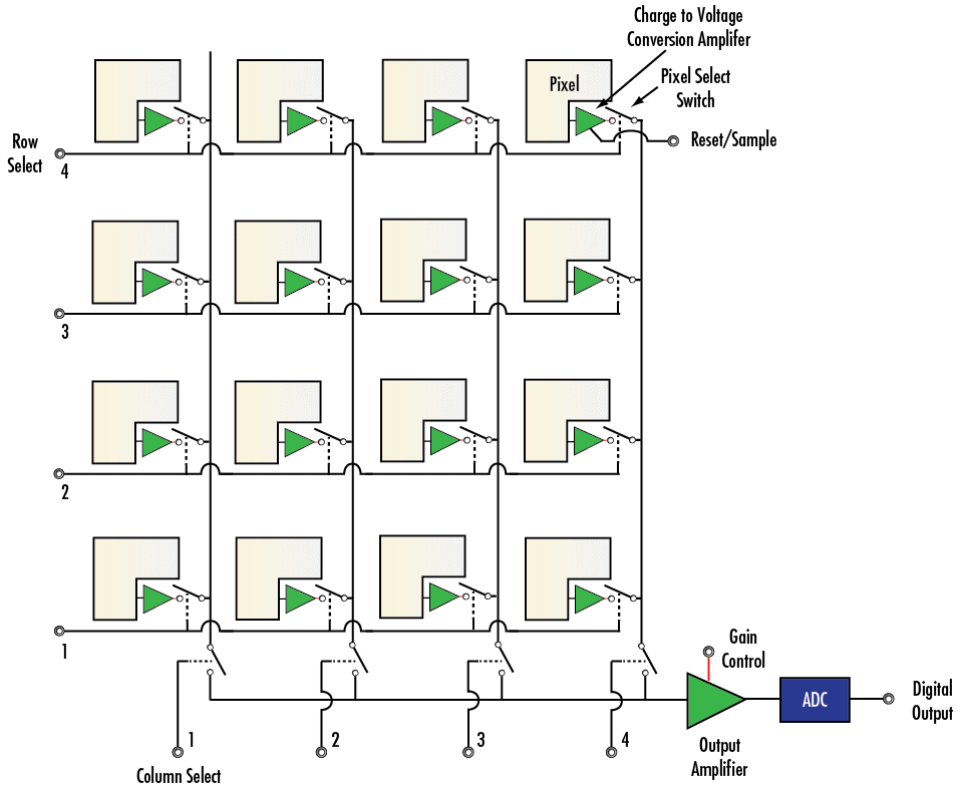

Figure 6. Block Diagram of CMOS Active Pixel Sensor (extracted from link).

2.4.2 Bayer Filter and Colour Sensitivity

Above the image sensor, the Bayer filter takes centre stage in capturing colour information. This filter is structured as a mosaic of colour filters, typically arranged in a repeating 2x2 pattern of red (R), green (G), and blue (B) filters. These filters are strategically positioned to capture the varying wavelengths of light associated with these colours. Importantly, the green filter is more abundant because the human eye is more sensitive to green light. This Bayer array thus captures a partial colour image by filtering light based on its colour composition.

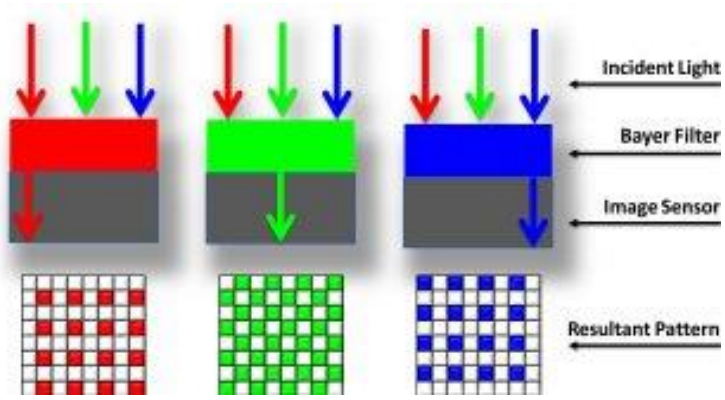

Figure 7. Bayer Layer Filter in CMOS sensors [30].

2.4.3 Near-Infrared (NIR) Filter and Spectral Range Expansion

In some camera configurations, an NIR filter is incorporated. NIR (Near-Infrared) filter in a CMOS image sensor is designed to attenuate or block light in the near-infrared spectrum, typically ranging from about 700 to 1000 nm, while allowing visible light, which spans roughly 400 to 700 nm, to pass through. This filter operates based on its spectral response curve, which quantifies its transmittance characteristics across different wavelengths.

By suppressing near-infrared wavelengths, the filter reduces the sensor's sensitivity to these higher-energy photons, preventing colour bleeding and spectral contamination. This, in turn, improves colour accuracy, minimises false colours, and optimises the image sensor's response to visible light. The NIR filter enables the camera to capture light in the near-infrared spectrum, which falls just beyond the range of human vision. This is particularly useful in applications like night vision, medical imaging, and material analysis. The NIR filter is designed to allow near-infrared wavelengths to pass through while blocking visible light. Its presence enhances the camera's versatility by providing access to information beyond the visible spectrum.

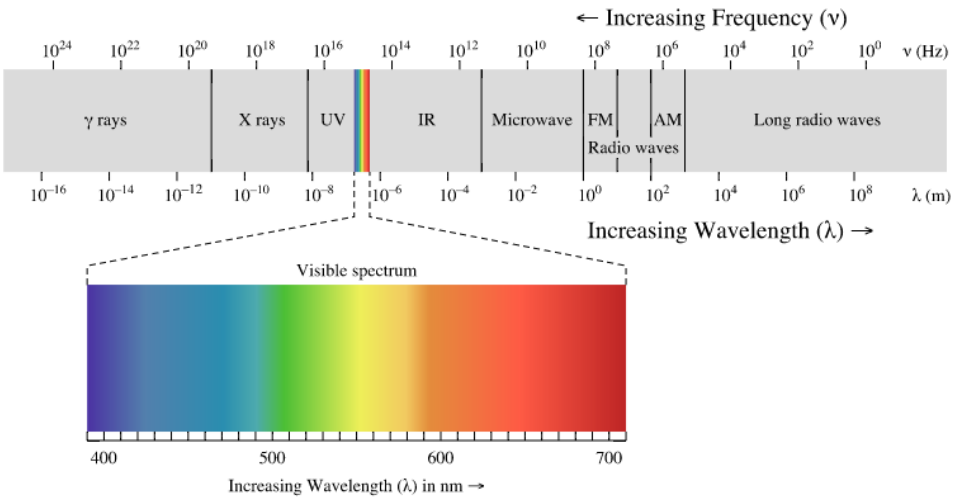

Figure 8. Visible Spectrum (extracted from link)

Throughout the camera's optical system, multiple layers of filters are positioned strategically to control the passage of light. These filters play a crucial role in shaping the spectral bandwidth of light that reaches the image sensor. Some filters transmit specific wavelengths, allowing them to contribute to the image, while others reflect or absorb unwanted wavelengths. The complexity of these filters lies in their ability to selectively transmit light while minimising distortions and artifacts.

2.5 LabGym for Behavioural Annotations

LabGym's workflow, shown in Figure 9, begins with background subtraction from each frame to isolate the animal. Data extraction at every video frame includes two types: "animation" data, representing the entire time window, and "pattern image" data, illustrating the animal's changing positions within the animation. These data feed into the "Categorizer," the core of the system, equipped with a neural network for behaviour classification. The "Categorizer" comprises the "Animation Analyzer," "Pattern Recognizer," and "Decision Maker" components.

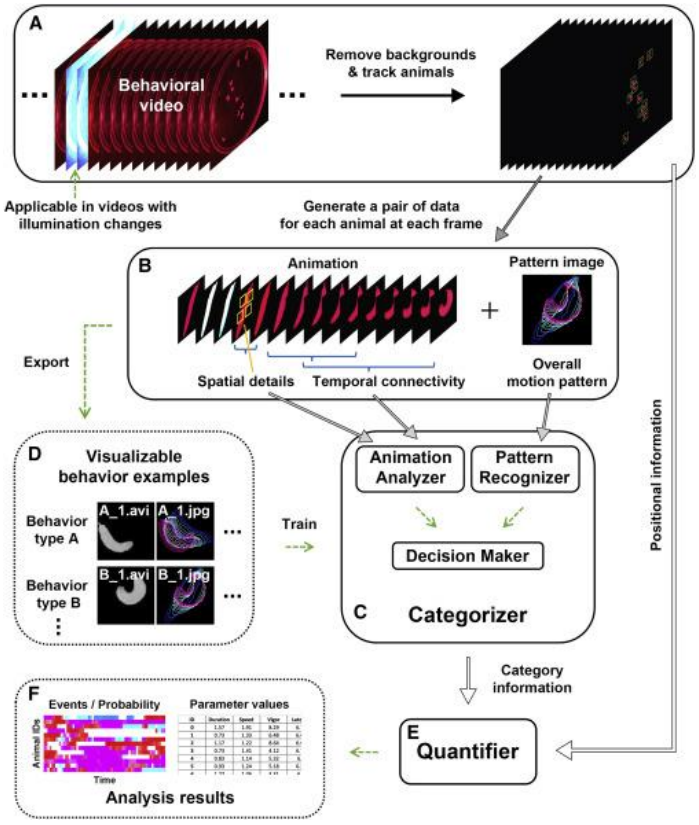

Figure 9. The pipeline of LabGym [31]

2.5.1 Animation Analyzer

It involves convolutional blocks combined with time-distributed layers, followed by recurrent layers. This model accepts 4-dimensional tensors (timestep, width, height, colour channel) as input. The neural network's results are subsequently transmitted to the Decision Maker.

2.5.2 Pattern Recognizer

The architecture in each level of the Pattern Recognizer mirrors that of the Animation Analyzer, with the key distinction being the absence of a time-distributed layers.

2.5.3 Decision Maker

The Decision Maker module is composed of three components: a concatenation layer, followed by two fully connected (dense) layers. The concatenation layer combines the outputs from both the Animation Analyzer and Pattern Recognizer, producing a unified 1D vector that feeds into the first dense layer. This first dense layer then connects to the second dense layer, where a SoftMax function is employed to calculate the probabilities associated with all behavioural categories.

2.5.4 Train Categorizers

The loss function applied for training the Categorizers is chosen based on the number of behavioural categories. Specifically, binary cross-entropy is used when there are two behavioural categories, while categorical cross-entropy is employed when there are three or more behavioural categories [31].

3 Methodology

3.1 Present Operational Frameworks

These were the present operational frameworks in the laboratory, at the start of this study. The aim was to utilise these frameworks to understand their weaknesses and overcome them.

3.1.1 Olympus SZX12 microscope

The Olympus SZX12 microscope coupled with the Scion CFW-1310M digital camera which has been in use encounters several significant challenges that warrant attention. The Scion CFW-1310M, a monochrome digital camera, appears to have a few shortcomings that make it less suitable for tasks involving video data capture. The first thing seen is that the camera comes equipped an IR filter and a spectral response that lies within the visible wavelength of lights as shown in Figure 10. This study involves the utilisation of blue and red LEDs which are from 450 to 495 nm, and 620 to 700 nm. Therefore, it is seen from the camera's spectral response that this will prove to be suboptimal in optogenetic stimulations.

Secondly, there is a very big issue of Field of View (FOV). The image senor architecture constrains the FOV (diagonal FOV ~20 mm) such that, manual calibration of the petri dish is required in real time. This means, moving the petri dish during the experiment to allow the camera to capture the movement of the larvae when they move out of frame. This greatly reduces the throughput and does not scale to the ideal parallelisation that is required. Another major issue becomes the real-time video

inspection on a computer. Although, it would not present an issue whilst training an AI model, the real time analysis presents a low frame rate output that is very laggy and jittery.

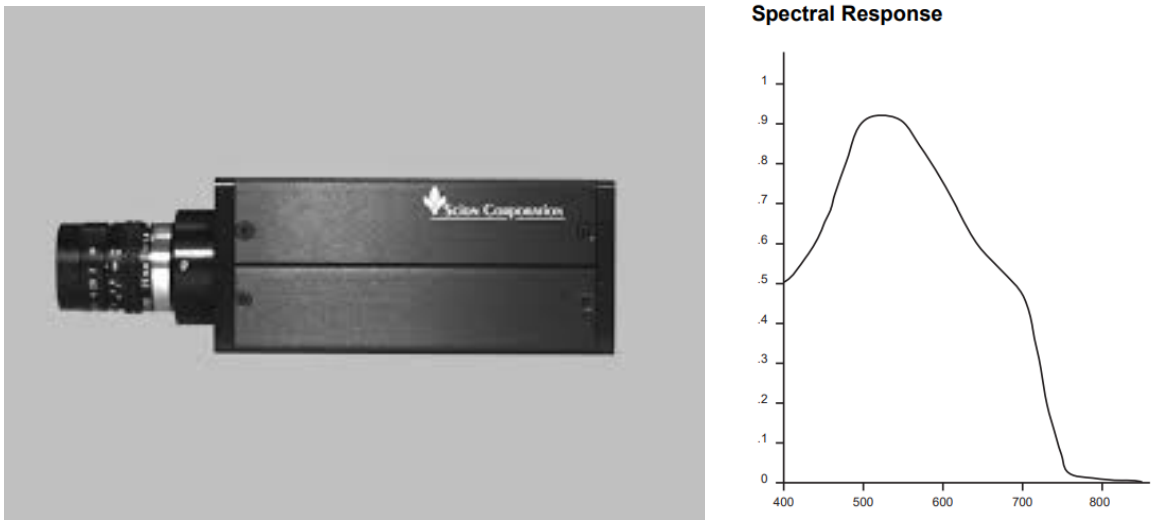

Figure 10. of Scion CFW-1310M and Spectral Response (link).

Considering these shortcomings, it becomes evident that the prevailing method apparatus falls short of providing an optimally conducive platform for our experimental endeavours. Addressing these issues is imperative to ensure not only the integrity of our scientific investigations but also to enhance the overall efficiency and effectiveness of our laboratory practices.

Figure 11. Example video collection using Scion CFW-1310M - showing low FOV (larva about to move out of frame)

3.1.2 Digicam LCMOS 3M coupled with Digicam CCTV Adapter

The Digicam LCMOS 3M coupled with the Digicam CCTV Adapter presents several problems that provides for suboptimal video collection. The first issue that is apparent from the get-go is the inherent dependence on a microscope, as these cameras act as extensions to already present

microscope. The same issue is seen in this system, wherein the spectrum of this camera lies in the visible light wavelengths and proves to be futile in optogenetic stimulations. The FOV issue is seen here again, wherein the camera presents a diagonal FOV of about 25 mm, which cuts the larvae when they move out of frame, as seen in Figure 12.

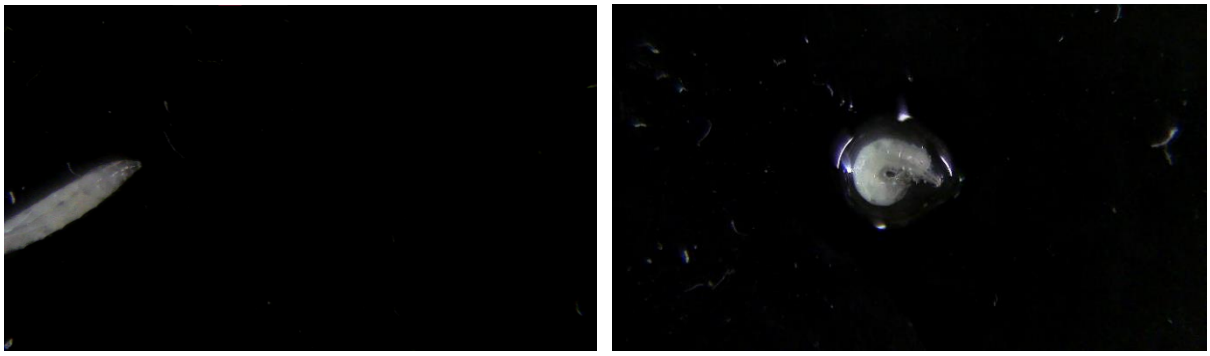

Figure 12. Example video collection using LCMOS 3M with CCTV lens - showing low FOV (larva out of frame in the left image)

3.2 Deciding Parameters for framework

3.2.1 FOV

Previous discussions have led to the decision of an ideal FOV. The most optimal camera and lens architecture would be the one that can be individually zoomed into the animal i.e., the larva with minimal undesirable frames (~35 mm diagonal FOV) and have a higher diagonal FOV bound to be able to incorporate the entire petri dish (either 60 mm or 90 mm).

3.2.2 Illumination

The illumination should be one that can be used to easily illuminate the entire and should be able to reveal intrinsic characteristics to allow for high contrast dark field video collection. This helps ensure that background subtraction can be performed easily. As discussed before, the stimulation spectrum of Chrimson and ChR2 reveal their spectrum to be between 450 nm and 650 nm. At these wavelengths, a camera with an IR filter will present an issue of glare, where the incident light on the petri dish reflects back into the camera. To avoid this issue, a sensor with no IR filter is needed, which is later applied in section 3.7. Therefore, this conducts that the illumination source should be in the

IR region, so that when a NoIR camera is coupled up with an IR filter to allow only the IR region wavelengths to pass, the illumination source seems visible to the camera.

3.2.3 Throughput

A higher FOV ensures that multiple larvae can be put in a petri dish for a mass exposure to the stimulation light and can be used to perform high throughput screening in parallel. This can be done by using 9 or multi-well petri dish plates, or multiple animals in a single petri dish.

Figure 13. Multi-well Plates (extracted from link).

3.3 Methods for Video Collections

The retrieval of third instar larvae, typically occurring around 96 hours post-egg laying, involved a gentle process. This entailed delicately squirting tap water into the soft fly food containing the larvae. It's essential to note that wandering larvae, those that had exited the food, or ones that had exhibited everted anterior or posterior spiracles, fell outside the suitable criteria for this assay due to their size or age.

To proceed, the contents of the soft fly food were transferred into a clean standard-sized Petri dish (measuring 100 mm x 15 mm). Forceps were employed to separate mid third instar larvae of medium size from smaller counterparts (second instar and early third instar) or larger larvae (late or wandering third instar). This separation process was carried out with utmost care to avoid any potential harm to the larvae's tissue. It's crucial to emphasise that the transfer using forceps primarily relied on water tension and not on applying pressure to the larvae using the forceps' blades. Alternatively, soft paint brushes could be used for manoeuvring the larvae. Regardless of the tool chosen, practice was

advisable to prevent unintended tissue damage that could complicate subsequent behavioural measurements.

Next, the mid third instar larvae were transferred, utilising forceps, into a smaller Petri dish (measuring 30 mm x 15 mm). This smaller dish contained a small plug of fly food moistened with water at room temperature. The larvae were kept in this smaller dish until the experiments were conducted, ensuring that this period did not exceed 20 minutes. Generally, transferring 20–30 larvae to the food plug provided an adequate number for conducting 20 minutes of behavioural assays.

For optimal visualisation, a mid-third instar larva (using forceps) was placed onto a thin pad of black or dark vinyl under a bright field stereomicroscope. The dark colour of the pad provided contrast, enhancing the visibility of the larva. It was recommended to use a piece of dark vinyl that could move freely, allowing precise alignment of the larva without physical contact.

The illumination sources were positioned between the microscope objective lenses and the black or dark vinyl pad to ensure adequate high-contrast illumination for observing the larva. Any excess water surrounding the larva, which might cause it to float on the vinyl pad, was wiped away using a paper towel. Lastly, the larva was oriented by adjusting the dark vinyl pad so that the larva's head/mouth pointed to the left for right-handed individuals and vice versa for left-handed individuals. Any larvae that did not exhibit normal locomotion after the transfer to the pad were discarded from the assay.

3.3.1 Mechanical nociception assay

The designated mechanical probe was applied, typically over a duration of 1–2 seconds, to the posterior dorsal side of the larva, around abdominal segment A8 shown in Figure 14. This action continued until the probe exhibited bending and generated a certain pressure level. It remained critical that the probe exerted pressure against the larva's dorsal surface, causing compression into the underlying pad at the point of contact.

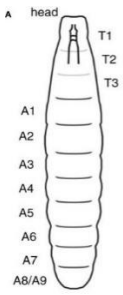

Figure 14. Body Segments of Drosophila Larva.

In cases where the tip of the nitinol filament met the dorsal cuticle-epidermis, probes with pressures below 2,300 kPa primarily experienced bending without penetrating the cuticle and underlying tissues. Such probes seldom had any noticeable impact on larval mortality. However, when pressures exceeded 5,000 kPa, the probes displayed both bending and, on occasion, penetration through the cuticle and underlying tissues. Larvae punctured by the probes exhibited impaired survival and were typically excluded from subsequent behavioural analysis.

Every larva's behavioural response was documented. A positive nociceptive response was recognised when the larva executed a full 360˚ roll along its body's axis within a 3-second timeframe. Conversely, other responses such as attempts to turn, rapid crawling, and wiggling were classified as negative for the purposes of this assay.

3.3.2 Chemical nociception assay

A concentrated stock solution of HCl (Sigma: 37.5–38.5%) was initially diluted to 10% concentration, assuming the original stock was at 37%. Subsequently, this 10% stock was further diluted with MilliQ water, resulting in a range of HCl solutions spanning from 0.5% to 9%. The exposure of a particular solution to the larvae was carried out by pipetting 1.5 µl of the respective HCl dilution onto a dish. The larvae were then allowed to explore the dish for approximately 10 seconds before being subjected to the chemical stimulus.

To ensure the reliability of the behavioural response data, certain precautions were taken. Larvae that reached the dish's wall were gently redirected back to the centre before the application of the chemical stimulus. Additionally, if the pipette tip came into contact with a larva, the behavioural

response of that specific larva was excluded from the analysis. This measure aimed to prevent any response from being influenced by a combination of physical touch and exposure to the acid.

In terms of behavioural assessment, a larva exhibiting a complete 360° roll along its body axis within 10 seconds of HCl exposure was recorded as displaying aversive behaviour. Other responses, such as fast crawling, turning, or bending, were not classified as aversive for the purposes of this assay. It's important to note that each larva was evaluated behaviourally only once to maintain consistency in the analysis.

3.3.3 Optical Nociception assay

The Blue or Red LED was illuminated based on the ontogenetically modified status of the larvae, maintaining an optimal distance of 16 cm (as determined through photodiode calculations) for a duration of 5 seconds. Subsequently, the behavioural responses exhibited by each larva were documented.

In terms of behavioural assessment, a positive nociceptive response was recognised if a larva executed a full 360˚ roll along its body axis within a 3-second timeframe following LED illumination. Conversely, other responses such as attempts to turn, rapid crawling, or wiggling were not categorised as nociceptive responses for the purpose of this assay. It is noteworthy that each larva was subjected to behavioural evaluation only once, ensuring consistency in the analysis.

3.4 Sony IMX477: Raspberry Pi HQ Camera

To replace the current operational frameworks, present in the lab, a Raspberry Pi was selected to create a prototype for video collection of the *Drosophila* experiments. The rationale behind the choice was its inherent availability and specifications discussed below.

The IMX477 is a 12.3 Mega-pixel CMOS active pixel type stacked image sensor featuring a diagonal measurement of 7.857 mm (Type 1/2.3) and a square pixel array. This sensor employs a mosaic filter with R, G, and B pigment primary colours, and it incorporates an electronic shutter with

adjustable integration time. Furthermore, it operates with three distinct power supply voltages: 2.8 V for analogue, 1.05 V for digital, and 1.8 V for input/output interface, all while maintaining low power consumption. The key specifications are mentioned in Figure15. We see that the camera is very sensitive to red light around the 600 nm wavelength, which later proves to be suboptimal for optogenetics.

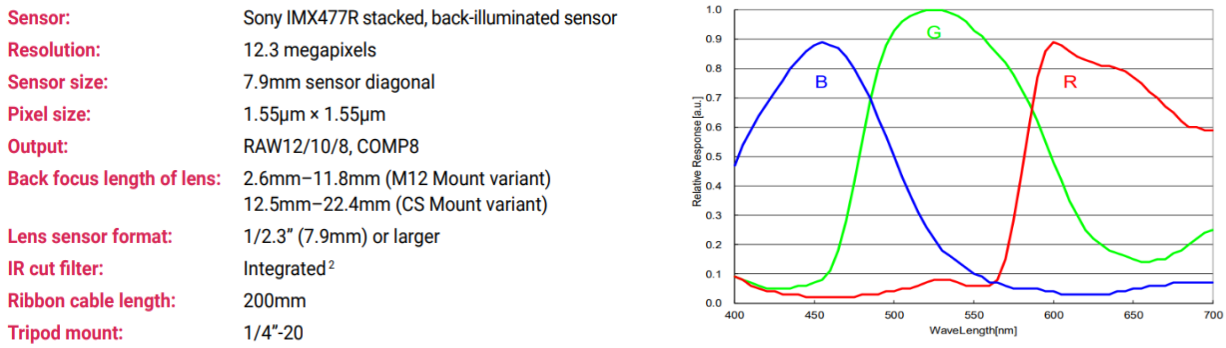

Figure 15. Specifications of IMX477 and Spectral Sensitivity (extracted from link)

3.5 Camera Lens Decision

3.5.1 Telephoto 16 mm

The prototype design commenced with the utilisation of an existing lens available in the laboratory, namely the Telephoto16 mm PT3611614M10MP lens. This lens features a 10-megapixel resolution and a fixed focal length of 16 mm, with an adjustable aperture ranging from F1.4 to F16. To incorporate it into the setup, calibration was performed, and it was attached to the Raspberry Pi HQ camera lens using a C-mount. Following the calibration process, this lens was used to capture videos from the recommended minimum object distance (MOD) of 0.2 meters, as specified in the datasheet. During this testing phase, various issues were observed.

As discussed previously, it's important to note that this sensor is equipped with an IR filter, rendering it unsuitable for scenarios where the illumination source is infrared (IR). Consequently, a white LED light source was employed to illuminate the petri dish from both sides. These LEDs were

positioned slightly above the petri dish surface, at approximately 3 cm, and were angled at 45 degrees from two sides to ensure even illumination, shown in Figure 16.

Figure 16. Prototype for testing Telephoto Lens

A number of challenges emerged within this system configuration, primarily centred around the choice of the camera lens. The 16 mm telephoto lens, positioned at a distance of 0.2 meters from the petri dish, and featuring a fixed 16 mm focus, calculates a diagonal field of view (FOV) of 99mm using the following formula:

$$\theta = 2 \times \tan^{-1}\frac{c}{2f} \quad (1)$$

$$Diagonal\ FOV = 2s \times \tan^{-1}\frac{\theta}{2} \quad (2)$$

Here, θ represents the angle of view, s is the MOD, c denotes the crop factor, and f stands for the focal length.

One significant limitation inherent in a fixed focal length lens is its incapacity for zoom adjustments to capture individual larvae in greater detail. This restriction can be particularly constraining when dealing with diverse subjects or scenarios requiring varying levels of magnification. Furthermore, when employing a 60 mm petri dish, the field of view provided by the 16 mm lens results in a surplus of unnecessary space surrounding the petri dish. This excess area can be impractical, especially when the goal is to focus exclusively on the contents within the dish.

Additionally, it's worth noting that the lens had its aperture settings previously adjusted for a different application, making it suboptimal for the specific requirements of the current task.

3.5.2 Microscope Lens for Raspberry Pi HQ Camera

Before proceeding further, the exploration of an alternative lens option was undertaken, specifically, the Microscope Lens designed for Raspberry Pi. This particular lens offered the feature of variable focus, spanning a working range from 45 mm to 135 mm. Furthermore, it facilitated the adjustment of magnification, ranging from 0.12X to 1.8X, with magnification ratio of 15:1.

Applying the same formulae as mentioned earlier for the IMX477 sensor paired with the Microscope Lens, the resulting analysis revealed that the diagonal field of view (FOV) at the recommended minimum object distance (MOD) of 0.05m ranged from 8.78 mm to 2.93 mm. However, as discussed in previous sections, it became evident that this FOV range did not align with the optimal requirements for video collection of the larvae due to the imposed constraints. Consequently, the research was continued to identify the most suitable lens configuration for the specific needs at hand.

3.5.3 FOV Calculation for optimal lens

Having already tested various lenses, at this point, vast research was conducted into the various lenses that are already available for the Raspberry Pi Camera. At this point, it was established that most of these previously tested cameras and operational frameworks fall short when it comes to variable FOV, and as such do not allow for calibrating the system to allow for obtaining a zoomed in video of the subject, or the whole video of a petri dish. This design constraint was kept in mind whilst conducting this research.

Before moving onto the results of this research, the sensor architecture of the IMX477 is detailed below to allow for FOV calculations. For the Sensor Diagonal measurement, the following formula was used:

$$Sensor\ Diagonal = \sqrt{Sensor\ Height^2 + Sensor\ Width^2} \quad (3)$$

$$= \sqrt{6.287^2 + 4.712^2} = 7.9\ mm$$

To calculate the crop factor of the camera relative to the 135-format (36x24 mm) film frame, the following calculations were done:

$$135\ format\ Diagonal = \sqrt{36^2 + 24^2}$$
$$= 43.26\ mm$$
$$Crop\ Factor = \frac{135\ format\ Diagonal}{Sensor\ Diagonal} \quad (4)$$
$$= \frac{43.26\ mm}{7.9\ mm}$$
$$= 5.477\ mm$$

This is summarised in the Table 1. Note, the camera mount available was C-mount camera, so it was given preference in the final decision of the lens architecture.

Camera Mount	C/CS
Sensor Name	SONY IMX477
Sensor Width (mm)	6.287
Sensor Height (mm)	4.712
Sensor Diagonal (mm)	7.9
Resolution (MP)	12.3
Pixel Size	1.55 µm x 1.55 µm
Optical Size	1/2.3"
Crop Factor	5.477

Table 1. Sensor Specifications useful for FOV calculations.

The calculation of the final diagonal FOV is done using the angle of view formula and the diagonal FOV formula discussed in equation 1 and 2, in section 3.5.1. The results of these calculations are shown in the table, with key specifications of the lens architecture.

As discussed in section 3.2.1, the DFOV needs to be between ~35 mm and 90 mm. Therefore, a variable focal length lens is the one that would be the most preferable. If not possible, then the second

option would be to opt for a lens whose DFOV is only minimally higher or lower than the petri dish. This would be a little inefficient if the case required for a single shot zoomed in detection of one larva inside the petri dish, however, it would still perform well when the larva is observed with all the surroundings. Upon the conduction of this research, several candidates were shortlisted to be applicable in both cases.

Lens Architecture	Image Format	Focal Length (mm)	Aperture	MOD(m)	HFOV (mm)	VFOV (mm)	DFOV (mm)
6mm Wide Angle	1/2"	6	F1.2	0.2	219	146	263
16mm Telephoto	1"	16	F1.4-1.6	0.2	82.2	54.8	99
Arducam 120°	1//1.7"	3.2	F2.0	0.3	616	411	741
50mm C-mount	2/3"	50	F1.8-16	0.5	65.7	43.8	79
8-50mm C-mount	1/2.3"	8-50	F1.4	0.2	164-26.3	110-17.5	197-31.6
2.8-12mm C-mount	1/2"	2.8-12	F1-1.6	0.3	704-164	469-110	846-197
35mm C-mount	2/3"	35	F1.7-16	0.2	37.6	25	45
5mm C-mount	1/1.7"	5	F1-1.6	0.15	197	131	237
8mm C-mount	2/3"	8	F1-1.6	0.15	123	82.2	148
8mm	1/1.7"	8	F1.8	0.3	246	164	296
25mm	1/2"	25	F2.4	0.3	78.9	52.6	95
M12 20 °	1/2.3"	25	F2	0.2	52.6	35.1	63

Table 2. DFOV calculations of multiple lens candidates

Shown in the Table 2, we see that the rows highlighted in green prove to be the most optimal choice. Others either have a very high DFOV (6 mm Wide Angle, Arducam 120°, 2.8-12 mm C-mount, 5 mm C-mount, 8 mm C-mount, 8 mm) or considerably lower DFOV (50 mm C-mount, 35 mm C-mount). The orange highlighted lens architectures are the ones that have an M-12 mount and would require an adapter to be connected to the present raspberry pi HQ camera.

From the green highlighted options, we can see that only one option offers a variable focal length, whereas others are fixed focus. From the fixed focus ones, the two orange highlighted options at the bottom are a good fit for an M-12 mount camera which can be used for constant FOV video collections of larvae in either 60 mm (M12 20° lens) or 90 mm (25 mm lens, 15 mm Telephoto). As

stated above, with the availability of a variable focal length, C-mount and a DFOV range of 197 mm to 31.6 mm, encompassing the two petri dish diameters and the need for a zoom of larvae, the 8-50 mm C-mount Lens, shown in Figure 16 was selected as the perfect fit.

Figure 17. 8-50 mm C-mount Lens

3.6 Prototype for 8-50 mm C-mount Lens

After the decision of the lens, the next step was to create a prototype for the system that would collect the experimental videos. This meant that there was a need to understand the relative positions and distances of each element of the design, namely the distance between the camera and the petri dish (dictated by the minimum MOD) and the distance between the incident stimulation led for optogenetics and the larva (S_{LL}). Before heading on with the schematics of the prototype, power density of the red LED was calculated at various S_{LL}.

3.6.1 Photodiode (GE) for calculating LED Power Density and S_{LL}

The power of the incident red stimulation light source was determined using a germanium photodiode PM16-122. Depending on the specific requirements for stimulating particular neurons, the goal was set to allow the S_{LL} measurement to conform to low-to-medium intensities (2 μW/mm²) and high intensities (22 μW/mm²) for Chrimson channelrhodopsin [32].

The recorded measurements were done whilst keeping the incident LED at a 45° angle and the beam was focused on the photodiode surface. The surface was a flat top, and the beam shape was circular. Keeping these two parameters constant, the values obtained are discussed in Table 3.

S_{LL} (cm)	Ambient Light Power (µW)	LED Power (µW)	Beam Shape	Beam Diameter (mm)	Beam Area (mm^2)	Power Density (µW /mm^2)
21	20	2180 ± 20	Circle	40	1256.63706	1.7347
18	25	2990 ± 25	Circle	34	907.92028	3.2932
16.5	18	3150 ± 18	Circle	30	706.85835	4.0420

Table 3. Power Density calculation using Photodiode.

These measurements allowed for precise characterisation and control of the stimulation light intensity, ensuring it met the requirements for stimulating specific neurons as dictated by the experimental goals. It is evident that the power density increases as we move closer to the photodiode. This is shown in Figure 18.

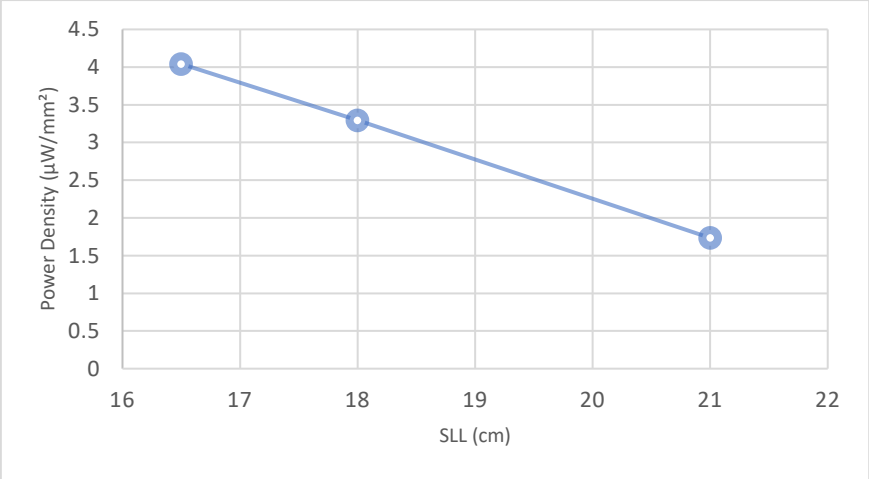

Figure 18. Graph of the Power Density and S_{LL} relation.

This helped decide that the low-to-medium intensity (2µW/mm^2) S_{LL} would be above 20.5 cm from the base of the petri dish and, moving closer to the petri dish will increase the power density of the incident beam of red LED. With the FOV constraint set and the S_{LL} distance set, the next step was to create a schematic of the 8-50 mm Lens video collection system.

3.6.2 Schematic of the Prototype-I

The schematic was initially crafted using Adobe Photoshop, with careful consideration given to adhering to the specified design constraints. Below, an image of the initial prototype is provided for reference, shown in Figure 19.

In this design, the 8-50 mm camera lens is positioned at a fixed distance of 20 cm from the base of the petri dish. This alignment precisely meets the Minimum Object Distance (MOD) requirement, guaranteeing a Diagonal Field of View (DFOV) range spanning from 197 mm to 31.6 mm.

Additionally, the placement of the red LED, intended for optogenetic applications, is set at a distance of 15 cm from the larvae. This configuration ensures that the power density is sufficient for accurate stimulation and the display of NEL responses.

Regarding the white illumination source, it is configured to provide even illumination to the petri dish from both sides at an angle of ~ 45° and a height of ~ 3 cm. This careful setup guarantees optimal lighting conditions for the experimental arrangement.

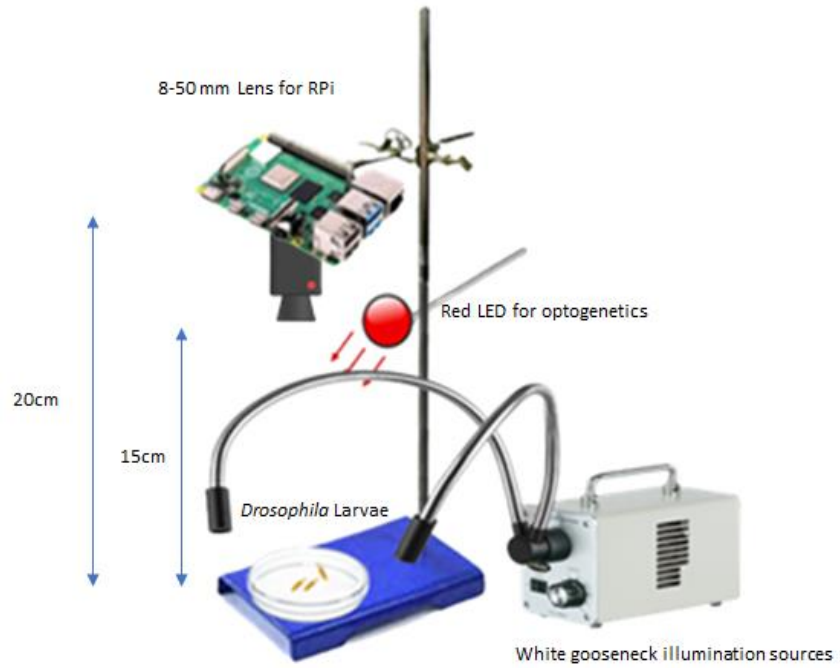

Figure 19. Schematic of Prototype-I with 8-50 mm Lens

This system was then implemented in the lab for real-time analysis and collection of video experiments. This was done through the CLI to record 60 second videos in the H264 format, whilst keeping the FOV of the camera to be enough to keep ~80% of the petri dish in the frame, exposure to ensure enough contrast between the background and the larvae, and illumination to make the larvae brighter than the background.

The command used was:

```
1. libcamera-vid -o test_name.h264 -t"time_ms" –width "width" height "height"
2. MP4Box -add test_name.h264 -fps "fps" test_name.mp4
```

Here, libcamera-vid is the library being utilised to record a video called “test_name”, for time “time_ms” in milliseconds, and with a resolution of “width” and “height”. That video is then converted to an mp4 format video using the library MP4Box, wherein we give it the input video in h264 format and provide the FPS configurations, and it outputs the converted video.

3.6.3 Red Beam Reflection Issue

The camera proved excellent in regard to the deciding parameter “FOV”. Using it, videos were collected with the whole petri dish in frame, 80% petri dish in frame and zoomed into the larvae as well (shown in Figure 20).

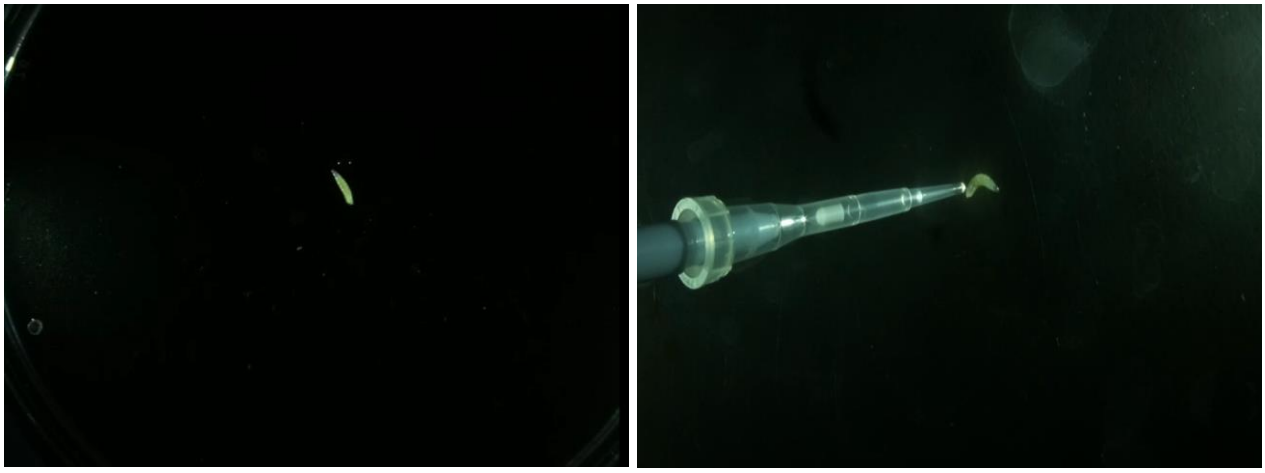

Figure 20. Video Stills from Prototype-I showing Chemical Nociception (Right)

This method proved excellent for chemical nociception, as there was no effect on illumination. Two concentrations of HCL were used, 8% HCL and 10% HCl. The data was collected using the above-mentioned commands and then stored into relevant folders.

For the 10% and 8% HCL nociception, 10 videos each were collected using the method in the section 3.3.2. Each experiment involved, one larva inside a 60 mm petri dish, which was allowed to move for 10 seconds and then stimulated. Out of these 10 larvae, 4 for the 10% HCL solution and 2 for the 8% HCL solution exhibited NEL.

Next, the system was setup to be used with the red LED for optogenetically modified Chrimson larvae. Each larva was placed inside a 60 mm petri dish, and individually exposed to the red LED. This is where problem of red reflection was faced. When the larva is exposed to the red light at 15 cm, the larva exhibited NEL, but it was not possible to capture it on the camera due to the concentration of the LED beam and the reflection. This is shown in Figure 21.

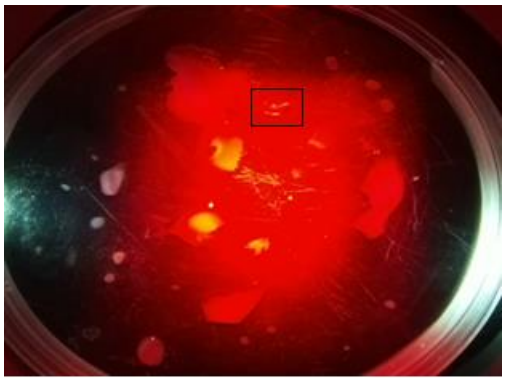

Figure 21. Red Beam Reflection Issue - shown in the black box is the larva.

In the black box, we can barely see the larva, as it is exhibiting NEL. This issue persisted throughout all the videos that were collected. The red LED was moved to a farther distance of about ~25 cm, to decrease the intensity of this issue but then the power density of the LED was not enough according to section 3.6.1, thus the larvae did not respond to the LED and no NEL was observed.

Afterwards, various exposure settings and illumination conditions were tried to remove this issue during collection but all of them failed.

3.6.4 Python Script for post-collection processing using OpenCV

An alternative technique was explored post-acquisition of the video dataset, entailing the utilisation of the cv2.split() function to subtract the red channel from the RGB image. This proved to be of no use. The ensuing step involved a grayscale conversion via the cv2.cvtColor() method for assessing its impact on the issue at hand. This again failed to provide a substantial enhancement in larva visibility.

Afterwards, another method was tried which involved the image undergoing a normalisation procedure using the cv2.normalize() function. Nonetheless, this approach did not yield a significant improvement in larva visibility. Subsequently, the next try was to binarise the image using the cv2.threshold() function, followed by an attempt to further refine clarity through the application of the cv2.adaptiveThreshold() method. A range of threshold values were iteratively explored, but none yielded the anticipated optimal outcome, resulting in the persistence of the unresolved issue.

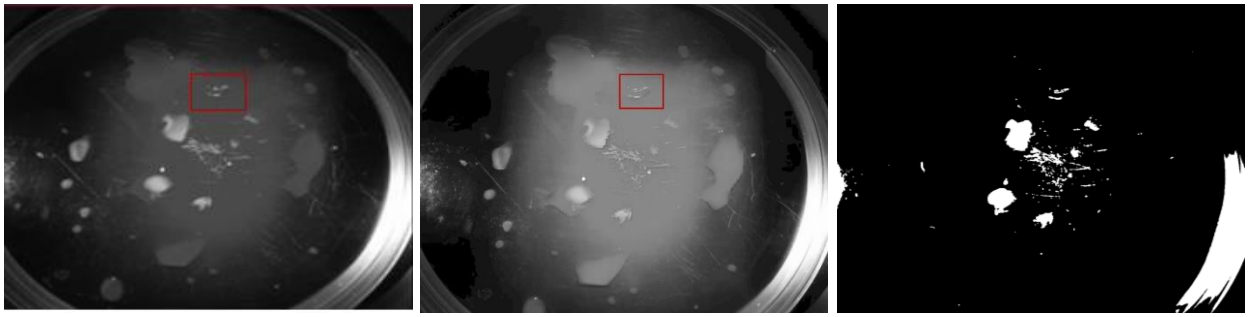

Figure 22. (Left) Image after Gray scaling, (Middle) Image after Normalisation, (Right) Image after Binary Thresholding - shown in red box is the larva.

3.7 NoIR Implementation

The presence of this issue necessitates consideration of the decision parameter outlined in section 3.2.2, specifically, a revision of the illumination conditions for the experimental setup. This means devising an approach that ensured the red LED light remained imperceptible to the camera's sensor. Given that the red LED light falls within the visible wavelength spectrum, the potential solution involves the implementation of an infrared (IR) filter to prevent the transmission of this light to the camera sensor.

However, it's imperative to note that the existing camera proves unsuitable for this purpose due to its inherent IR cut-off filter, which would hinder the effective filtration of the red LED light. Moreover, the consideration of employing a visible spectrum optical cut-off filter introduces a new challenge, as it would render the white illumination source for the experiments imperceptible to the

camera. Consequently, the entire frame would appear black until the red LED is directed towards the larvae, which presents a substantial drawback.

Both of these issues mean, that there is a requirement for a camera that has no IR filter, thereby ensuring that when an IR filter above the visible spectrum is coupled with the camera, the red LED can not pass through to the camera. Furthermore, this necessitates the use of IR LEDs to illuminate the larvae, so that the only light passing through to the camera is the illumination of the larvae and no interference.

3.7.1 Prototype for NoIR Camera: Sony IMX708

To address this need, the camera model selected was the NoIR version of the v3 camera module for Raspberry Pi. It comes with no IR filter, thereby allowing IR region of the spectrum to pass through to the sensor as well. The camera specifications are shown below in Figure 23, along with the spectral response of the sensor.

Sensor:	Sony IMX708
Resolution:	11.9 megapixels
Sensor size:	7.4mm sensor diagonal
Pixel size:	1.4µm × 1.4µm
Horizontal/vertical:	4608 × 2592 pixels
Common video modes:	1080p50, 720p100, 480p120
Output:	RAW10
IR cut filter:	Integrated in standard variants; not present in NoIR variants
Autofocus system:	Phase Detection Autofocus
Dimensions:	25 × 24 × 11.5mm (12.4mm height for Wide variants)
Ribbon cable length:	200mm
Cable connector:	15 × 1mm FPC

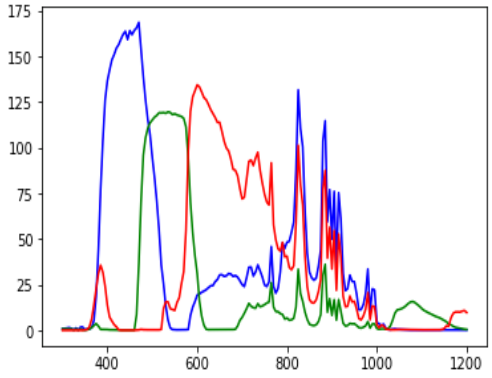

Figure 23. Specifications of IMX708 and Spectral Sensitivity from datasheet

This camera comes with a pre-attached lens, so there was no need to attach a new lens to the camera. There is a high response in the IR region seen in the spectral sensitivity, thereby ascertaining that this would be perfect for IR illuminated experiments. The FOV calculations of this camera were considered before it was chosen. The camera has Phase Detection Autofocus which is automatically adaptive. This means that the MOD (minimum 0.1m) can be moved, and the focus can be shifted. However, for the implementation in this case, it is desirable to have as many fixed variables as

possible, to ensure similar experiment collection conditions can be recreated. The camera also allowed for the control of contrast, exposure time and value, saturation, brightness etc.

The camera's focus was set to manual control using a python script and was iteratively tested using a for loop, to find the best possible focus at 0.1m from the base of the petri dish. This value and other parameters are discussed in section 3.7.5.

3.7.2 Long pass filter with IR LEDs

With the camera set, the next step is to couple it with an optical filter that allows for only wavelengths in the IR region to pass through. For this purpose, a 67 mm 720 nm pass IR filter is chosen. This means that the IR filter will only allow for light in the region of 720 nm and more to pass through the filter and block the rest of the light, as shown in Figure 24. This would ascertain that the red light from the stimulation source does not pass through the filter. This necessitates the implementation of a new illumination source because the current light source falls in the visible spectrum being blocked by the filter, as shown in the figure below.

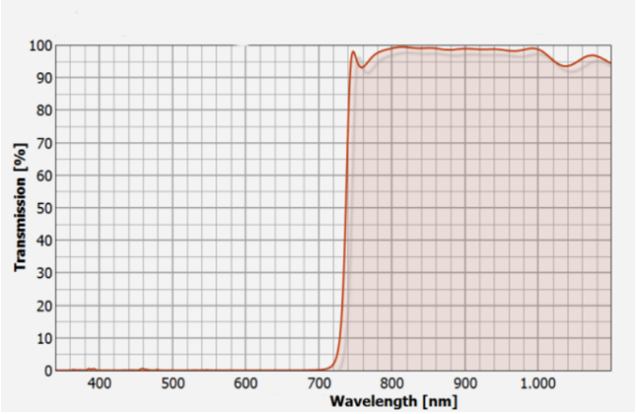

Figure 24. Spectral Sensitivity of 720 nm pass optical IR filter.

For this purpose, IR emitters were selected, with an illumination wavelength in the IR region, ideally around ~850 nm, to allow for ideal lighting conditions of the larvae. A quick circuit was patched up to allow for 3 of these emitters to be incident on the larvae from a 45° angle.

3.7.3 Schematic of the Prototype-II

This schematic design was created using Photoshop, and just like in section 3.6.2, the design constraints were taken into consideration during illustration. This design is shown in Figure 25.

In this design, NoIR camera is fitted at the bottom of the Raspberry Pi, using a plastic plate. This is positioned at a fixed distance of 10 cm from the base of the petri dish. This alignment ensures that the design meets the MOD requirement. The red LED is positioned at the same distance (15 cm from base) as in section 3.6.2, because of the power density constraints. The optical filter is positioned right below the camera to allow for maximum restriction of visible light wavelengths. The IR emitters are positioned at a 45° angle and a distance of ~5 cm from the petri dish, horizontally and vertically.

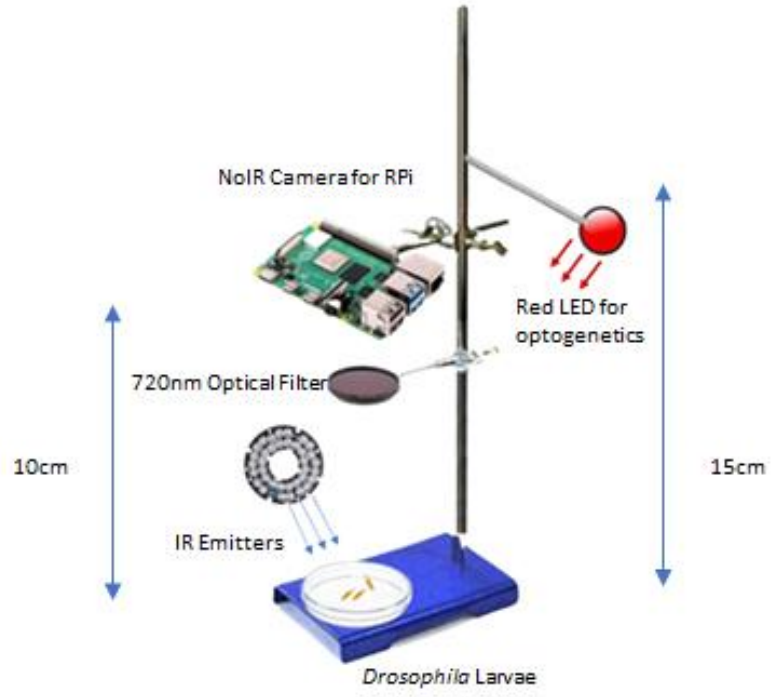

Figure 25. Schematic of Prototype-II with NoIR Camera

3.7.4 Measurement and video collection scripts in Python

Using this prototype, solved the issue of the red beam reflection that was present in the previous case. The IR emitters illuminated the larvae excellently and this allowed for the most optimal video collections. This is where the last design parameter was also implemented that is, throughput as discussed in section 3.2.3.

Having already solved the issue of FOV and illumination, this marked the completion of the design constraint. The NoIR camera's DFOV was adjusted to accommodate a 60 mm petri dish, ascertaining that the whole petri dish was in the frame. The IR emitters, positioned as shown in the design, were the only wavelengths passing through the optical filter. This meant that the red LED could be now used at the optimal distance of 15 cm from the larvae for video collection.

The setup was done according to the prototype, and multiple optogenetically modified Chrimson larvae were collected in a 60 mm petri dish. This was done in conformity of the optogenetic method for experimentation as in section 3.3.3. With multiple larvae in the petri dish, they were allowed to roam for 10 s, after which they were stimulated with the light source.

Given below are the images during the stimulation, showing that little to no red light was detected through the camera and the system presented the most optimal results yet. The image on the left shows the larvae before the stimulation. The image on the right shows very minimal red-light interference, which can be neglected.

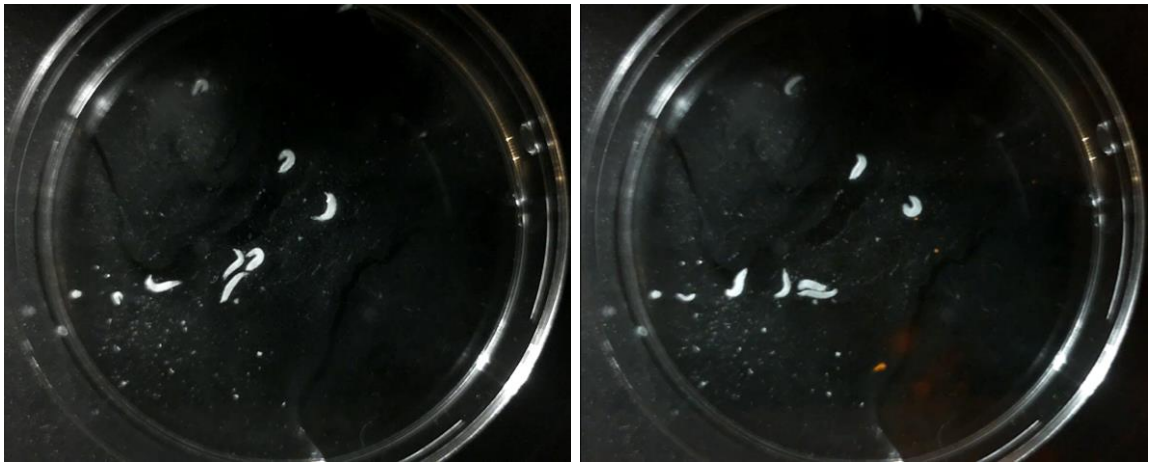

Figure 26. Perfect Video Collection with minimal red interference from Prototype-II.

With this, the prototype succeeded in implementing all the design constraints, whilst ensuring an efficient video collection method.

This was then used to collect 10 videos of optogenetically modified larvae, with 4 using the blue LED for ChR2 channelrhodopsin (same methodology and design) and 6 being with red LED for Chrimson channelrhodopsin.

The script used for collecting these videos was written in Python on a local Raspberry Pi IDE by the name of Thonny. It utilises a library called picamera2 which has advanced features to allow for the modification of camera parameters for the NoIR camera. It begins by asking the user for the file name to store the video, when the user enters the file name, a preview window is opened, and a 60 s recording begins. The user is reminded at 15 seconds with a prompt to start the LED stimulation, and after 5 seconds, a prompt is shown to stop the stimulation. This allows for a standardised timing of the incident LED to assure a constant response measurement time around the ~20 s to 30 s window in each video. The script then converts the video to an mp4 and stores it.

3.7.5 Camera parameters

The picamera2 library provides an excellent guide on how to change the camera parameters for the most optimal video collection.

3.7.5.1 Lens Position to focus at 10 cm

The first parameter that was kept constant was the focus of the camera. This was done by disabling the autofocus and then iteratively looping through different “LensPostion” values to find the most optimal focus, presenting a clear outlook at the minimum MOD. The lens position control, accessed via `picam2.camera_controls['LensPosition']`, provides three key values: the minimum, maximum, and default lens positions. The minimum value denotes the farthest focal distance achievable, while the maximum value specifies the closest attainable focal distance (computed as the reciprocal of this value). The third value represents the "default" setting, typically corresponding to the lens's hyperfocal position. The minimum lens position value is 0.0, signifying an infinite focal distance. A maximum value of 10.0 suggests that the nearest focal distance is 1/10 m or 10 cm. Therefore, at 10 cm the lens position was set to 10.

3.7.5.2 Exposure Time and Value

The exposure time parameter refers to the duration the sensor utilises, quantified in μs. Exposure compensation, measured in "stops," serves to modify the target of the AEC (Auto Exposure Control)

and AGC (Automatic Gain Control) algorithms. Positive values raise the target brightness level, while negative values lower it. A value of zero signifies the baseline or "normal" exposure setting. Various exposure settings were tested in company with the contrast values. The best values were obtained where the background of the videos was completely in contrast with the bright larvae. It was observed that the exposure time can be increased to a higher value, but then the value needs to be reduced to allow for optimal contrasts. The final value for Exposure was set to 0, whilst keeping the exposure time to 5000 μs.

3.7.5.3 Contrast

This function adjusts the contrast of the image. The upper and lower limits of contrast are floating point number 0.0 and 32.0 respectively. A setting of zero corresponds to "no contrast," 1.0 represents the default "normal" contrast, and higher values incrementally increase the contrast proportionally. Contrast was set according to the different conditions of exposure values and times. For the final setting, any value of contrast over 1 would cause one or more larvae to disappear and lead to suboptimal video collection.

3.8 LabGym Implementation

LabGym has an inbuilt larval nociception model built for 30 FPS detection. The model is trained over the same framework as discussed in the section 2.5. The model characteristics are discussed here.

```
Epoch 00024: val_loss did not improve from 0.14261
Restoring model weights from the end of the best epoch

Epoch 00024: ReduceLROnPlateau reducing learning rate
Epoch 00024: early stopping
              precision    recall  f1-score   support

    crawling       0.96      0.97      0.96      3430
     curling       0.95      0.95      0.95      3185
    immobile       0.99      0.96      0.97      2170
     rolling       0.95      0.96      0.95      3500
     turning       0.96      0.97      0.96      2905
   uncoiling       0.94      0.93      0.93      2310

    accuracy                           0.96     17500
   macro avg       0.96      0.95      0.95     17500
weighted avg       0.96      0.96      0.96     17500
```

Figure 27. Model Metrics - Larva Nociception Model using LabGym.

From Figure 27, we that the trained model has an accuracy of 96% for overall behavioural annotation. Here we are interested in the “rolling” behaviour of the larvae.

For rolling, the model exhibits a precision of 95%, which means that 95% of the predictions made for the behaviour rolling were true positives i.e., the larvae did roll. Furthermore, taking into account the recall it is observed that for 96% of the positive cases are predicted positive. This together gives the rolling behavioural annotation a very high f1-score of 95%. A high f1-score makes it certain that the model is not only good at one behavioural annotation, but shows the ability to identify negative cases, which in the case of rolling, would be any other behaviour.

Figure 28 shows the training history, and it is observed that over 20 epochs, the training accuracy increased significantly, and the training loss decreased considerably.

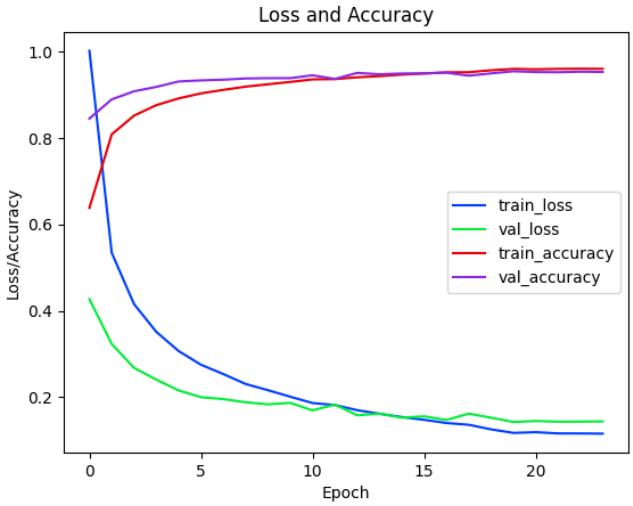

Figure 28. Training History for Larva Nociception Model

3.8.1 Inference using LabGym Larva Nociception Model

For the inference, a 1024 x 768 size video was initially chosen, the LabGym larva nociception model took 60.988 s time to subtract the background. The background subtraction result is shown in Figure 29.

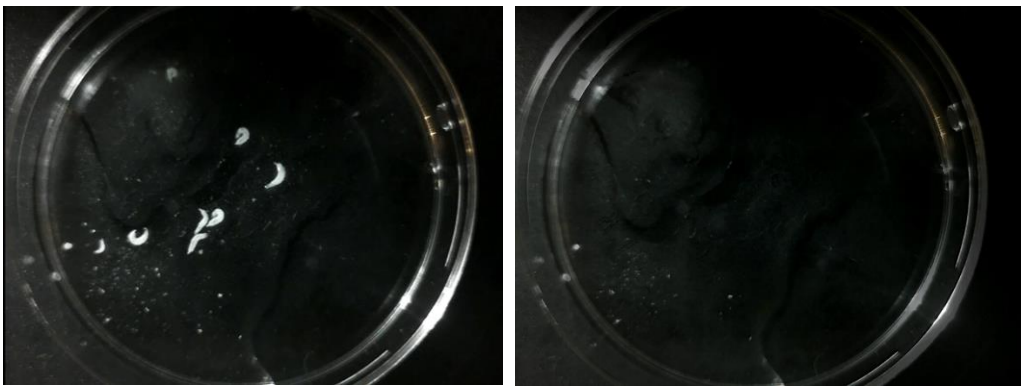

Figure 29. Background Subtraction from the left frame

The time to acquire information in 1000 frames was 185.964 s. The video annotation took 21.39 s. The video presented four larvae rolling, which was determined before running inference. These larvae were marked and then compared to the annotation by the model. The model showed a high accuracy on the very apparent NEL, and even on the less apparent NEL, it showed a 77% accuracy.

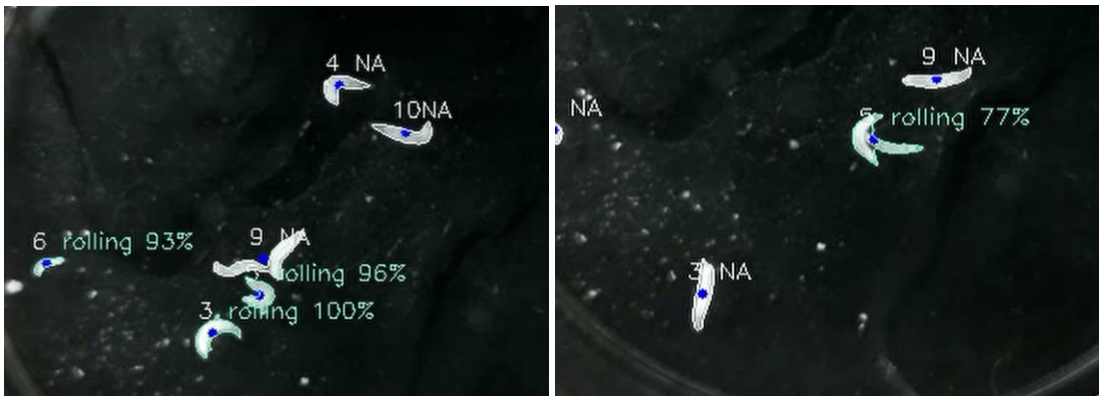

Figure 30. Model Correctly Annotating all NEL instances in the video.

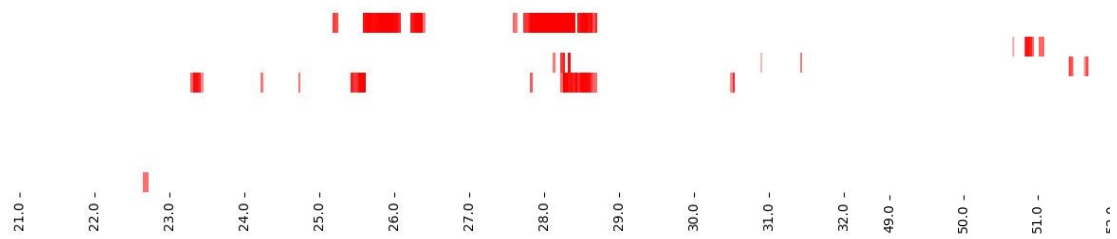

Figure 31. Behaviour Plot for three larvae, showing continuous rolling in red. Rolling is considered as NEL, when it is continuous over ~2 s. After time skip (picture cropped), the 4th larva also presents rolling. Here, x-axis is the time and y-axis are the larval number.

Next the video was down sampled to 640 x 480 size, the LabGym larva nociception model took 22.52 s time to subtract the background. The background subtraction results were the same with a considerable decrease in time. The time to acquire information in 1000 frames was 58 s. The video annotation took 21.946 s. The annotation took a similar time, but the time to acquire information from each frame was ~3x less. Further to that, the annotated videos showed the same results, and the 4 larvae were annotated correctly.

In another instance, the original video was down sampled to 480 x 360 size, the LabGym larva nociception model took 17.6 s time to subtract the background. The background subtraction results were the same with a smaller decrease in time. The time to acquire information in 1000 frames was 51 s. The video annotation took 16.2 s. However, this time one of the larvae which exhibited NEL, did not show up in the annotated video, as shown in the Figure 32.

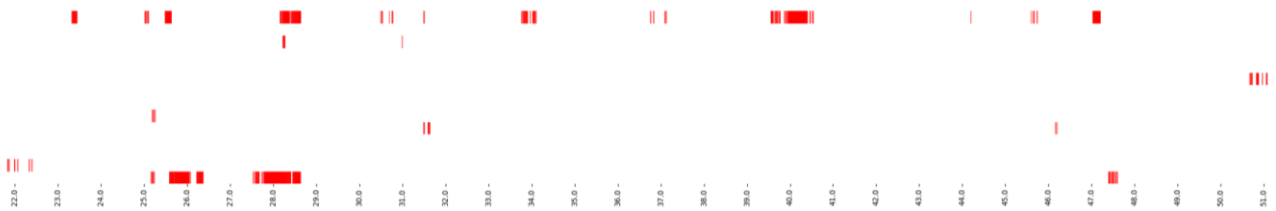

Figure 32. 3 (top, bottom, middle at 51 s) out of actual 4 larvae exhibited continuous rolling to be classified as NEL.

Therefore, it is observed that by down sampling the videos, we can decrease the time it takes for the model to run inference. This characteristic proves very useful for future usage where multiple larvae can be put in multi-well plates, and the videos can be cropped to run high speed inference on them.

4 Conclusion and Future Work

This study approached the problem systematically, beginning with a comprehensive review of existing frameworks and their limitations. Extensive research efforts were then dedicated to overcoming these limitations. Throughout the implementation process, three key design constraints influenced the selection of camera lenses and experimental conditions. These constraints not only informed the development of a second prototype but also shed light on the shortcomings of the initial one. Various methods were employed to maintain optimal experimental conditions consistently. The final design, Prototype-II, in conjunction with the highly precise LabGym model, successfully addressed the problem at hand.

One of the primary objectives from the outset was to establish an iterative pipeline that could be revisited and repeated in case of suboptimal data collection. This concept played a pivotal role in shaping the methodology. For instance, when confronted with the challenge of red reflection in the Raspberry Pi HQ Camera, the pipeline steps were retraced to explore a new camera architecture with similar field of view (FOV) calculations, potentially resolving the issue. This iterative approach guided the implementation through the pipeline, allowing for continuous refinement.

This study, along with its video collection methods and prototype schematics, is poised to make a substantial contribution to a significant grant for the Fruit Fly laboratory. The success of this project will greatly enhance the day-to-day research activities conducted in the laboratory. The design will streamline experimentation methods and subsequent data recording, enabling automated annotation of larval behaviour. Importantly, this approach has the potential to be applied beyond its current scope. The LabGym models can be adapted to train over any dataset with appropriate illumination conditions. Consequently, the methodology presented here could serve as a foundation for future dataset designs beyond *Drosophila*. All the gathered data, software code, and prototype schematics will be made accessible to the laboratory, facilitating a seamless transition from manual to automated annotation processes.

5 Bibliography

[1] T. D. Pereira *et al.*, "SLEAP: A deep learning system for multi-animal pose tracking," *Nat Methods*, vol. 19, no. 4, 2022, doi: 10.1038/s41592-022-01426-1.

[2] N. S. Tolwinski, "Introduction: Drosophila-A model system for developmental biology," *Journal of Developmental Biology*, vol. 5, no. 3. 2017. doi: 10.3390/jdb5030009.

[3] A. Del Valle Rodríguez, D. Didiano, and C. Desplan, "Power tools for gene expression and clonal analysis in Drosophila," *Nature Methods*, vol. 9, no. 1. 2012. doi: 10.1038/nmeth.1800.

[4] S. C. Miller, S. J. Brown, and Y. Tomoyasu, "Larval RNAi in Drosophila?," *Dev Genes Evol*, vol. 218, no. 9, 2008, doi: 10.1007/s00427-008-0238-8.

[5] A. Pavin, K. Fain, A. DeHart, and D. Sitaraman, "Aversive and Appetitive Learning in Drosophila Larvae: A Simple and Powerful Suite of Laboratory Modules for Classroom or Open-ended Research Projects.," *J Undergrad Neurosci Educ*, vol. 16, no. 2, 2018.

[6] F. Hirth, "Drosophila melanogaster in the Study of Human Neurodegeneration," *CNS Neurol Disord Drug Targets*, vol. 9, no. 4, 2012, doi: 10.2174/187152710791556104.

[7] F. Heigwer, F. Port, and M. Boutros, "Rna interference (RNAi) screening in Drosophila," *Genetics*, vol. 208, no. 3, 2018, doi: 10.1534/genetics.117.300077.

[8] C. Ong, L. Y. L. Yung, Y. Cai, B. H. Bay, and G. H. Baeg, "Drosophila melanogaster as a model organism to study nanotoxicity," *Nanotoxicology*, vol. 9, no. 3. 2015. doi: 10.3109/17435390.2014.940405.

[9] W. W. Smith, J. Thomas, J. Liu, T. Li, and T. H. Moran, "From fat fruit fly to human obesity," *Physiology and Behavior*, vol. 136. 2014. doi: 10.1016/j.physbeh.2014.01.017.

[10] T. C. Kaufman, "A short history and description of Drosophila melanogaster classical genetics: Chromosome aberrations, forward genetic screens, and the nature of mutations," *Genetics*, vol. 206, no. 2, 2017, doi: 10.1534/genetics.117.199950.

[11] K. Prüßing, A. Voigt, and J. B. Schulz, “Drosophila melanogaster as a model organism for Alzheimer’s disease,” *Molecular Neurodegeneration*, vol. 8, no. 1. 2013. doi: 10.1186/1750-1326-8-35.

[12] L. D. Sibley, “The roles of intramembrane proteases in protozoan parasites,” *Biochimica et Biophysica Acta - Biomembranes*, vol. 1828, no. 12. 2013. doi: 10.1016/j.bbamem.2013.04.017.

[13] J. H. Massey and P. J. Wittkopp, “The Genetic Basis of Pigmentation Differences Within and Between Drosophila Species,” in *Current Topics in Developmental Biology*, 2016. doi: 10.1016/bs.ctdb.2016.03.004.

[14] N. Fenwick, G. Griffin, and C. Gauthier, “The welfare of animals used in science: how the ‘Three Rs’ ethic guides improvements.,” *Can Vet J*, vol. 50, no. 5, 2009.

[15] H. R. Ferdowsian and N. Beck, “Ethical and scientific considerations regarding animal testing and research,” *PLoS One*, vol. 6, no. 9, 2011, doi: 10.1371/journal.pone.0024059.

[16] A. Singhania and W. B. Grueber, “Development of the embryonic and larval peripheral nervous system of Drosophila,” *Wiley Interdiscip Rev Dev Biol*, vol. 3, no. 3, 2014, doi: 10.1002/wdev.135.

[17] J. He *et al.*, “Drosophila as a Model to Study the Mechanism of Nociception,” *Frontiers in Physiology*, vol. 13. 2022. doi: 10.3389/fphys.2022.854124.

[18] Z. D. Marshall and E. S. Heckscher, “The Role of Even-Skipped in Drosophila Larval Somatosensory Circuit Assembly,” *eNeuro*, vol. 9, no. 1, 2022, doi: 10.1523/ENEURO.0403-21.2021.

[19] L. E. Cheng, W. Song, L. L. Looger, L. Y. Jan, and Y. N. Jan, “The Role of the TRP Channel NompC in Drosophila Larval and Adult Locomotion,” *Neuron*, vol. 67, no. 3, 2010, doi: 10.1016/j.neuron.2010.07.004.

[20] W. B. Grueber, B. Ye, A. W. Moore, L. Y. Jan, and Y. N. Jan, “Dendrites of distinct classes of Drosophila sensory neurons show different capacities for homotypic repulsion,” *Current Biology*, vol. 13, no. 8, 2003, doi: 10.1016/S0960-9822(03)00207-0.

[21] D. T. Babcock, S. Shi, J. Jo, M. Shaw, H. B. Gutstein, and M. J. Galko, “Hedgehog signaling regulates nociceptive sensitization,” *Current Biology*, vol. 21, no. 18, 2011, doi: 10.1016/j.cub.2011.08.020.

[22] T. L. Follansbee *et al.*, “Drosophila nociceptive sensitization requires BMP signaling via the canonical SMAD pathway,” *Journal of Neuroscience*, vol. 37, no. 35, 2017, doi: 10.1523/JNEUROSCI.3458-16.2017.

[23] C. Munnik, M. P. Xaba, S. T. Malindisa, B. L. Russell, and S. A. Sooklal, “Drosophila melanogaster: A platform for anticancer drug discovery and personalized therapies,” *Frontiers in Genetics*, vol. 13. 2022. doi: 10.3389/fgene.2022.949241.

[24] L. Kruger and T. T. Denton, “A standardized method for incorporation of drugs into food for use with Drosophila melanogaster,” *Anal Biochem*, vol. 599, 2020, doi: 10.1016/j.ab.2020.113740.

[25] A. Eriksson *et al.*, “Using Drosophila behavioral assays to characterize terebrid venom-peptide bioactivity,” *Sci Rep*, vol. 8, no. 1, 2018, doi: 10.1038/s41598-018-33215-2.

[26] X. Hao *et al.*, “The Effects of General Anesthetics on Synaptic Transmission,” *Curr Neuropharmacol*, vol. 18, no. 10, 2020, doi: 10.2174/1570159x18666200227125854.

[27] Z. Hamoudi, T. M. Khuong, T. Cole, and G. G. Neely, “A fruit fly model for studying paclitaxel-induced peripheral neuropathy and hyperalgesia,” *F1000Res*, vol. 7, 2018, doi: 10.12688/f1000research.13581.2.

[28] P. Mahmoudi, H. Veladi, and F. G. Pakdel, “Optogenetics, Tools and Applications in Neurobiology,” *Journal of Medical Signals and Sensors*, vol. 7, no. 2. 2017. doi: 10.4103/2228-7477.205506.

[29] E. S. Boyden, F. Zhang, E. Bamberg, G. Nagel, and K. Deisseroth, “Millisecond-timescale, genetically targeted optical control of neural activity,” *Nat Neurosci*, vol. 8, no. 9, 2005, doi: 10.1038/nn1525.

[30] O. S. Siordia, I. M. De Diego, C. Conde, and E. Cabello, “Wireless in-vehicle complaint driver environment recorder,” in *SIGMAP 2011 - Proceedings of the International Conference on Signal Processing and Multimedia Applications*, 2011. doi: 10.5220/0003567300520058.

[31] Y. Hu *et al.*, “LabGym: Quantification of user-defined animal behaviors using learning-based holistic assessment,” *Cell Reports Methods*, vol. 3, no. 3, 2023, doi: 10.1016/j.crmeth.2023.100415.

[32] D. Tadres and M. Louis, “PiVR: An affordable and versatile closed-loop platform to study unrestrained sensorimotor behavior,” *PLoS Biol*, vol. 18, no. 7, 2020, doi: 10.1371/journal.pbio.3000712.